Minimum thickness of semi-circular skewed masonry arches

Tamás FORGÁCS[a], Vasilis SARHOSIS[b], Katalin BAGI[a*]

[a] *Dept. of Structural Mechanics, Budapest University of Technology and Economics,*
tamasforgacs@hotmail.com; kbagi@mail.bme.hu
[b]*School of Civil Engineering and Geosciences, Newcastle University, Newcastle Upon Tyne, NE1 7RU, UK,*
Vasilis.Sarhosis@newcastle.ac.uk

Abstract

The problem of determining the minimum thickness of masonry arches has been a challenge to the engineering community through the last two centuries. Although significant work has been undertaken to investigate the minimum thickness of semi-circular and elliptical rectangular arches, no work has been done to investigate the minimum thickness of skew arches. In this paper we computed the minimum thickness of semi-circular skewed masonry arches when subjected to their self-weight. Using the Discrete Element Method (DEM), a sensitivity study has been carried out to investigate the minimal barrel thickness with respect to the: a) angle of skew; b) construction method (false, helicoidal, and logarithmic); c) size of masonry units; and d) frictional resistance between masonry units. The construction method and the angle of skew significantly influences the minimum barrel thickness of the arch. For skew arches constructed using the false method, as the angle of skew increases, the minimum barrel thickness increases. However, for skew arches constructed using the helicoidal and logarithmic method, as the angle of skew increases, the minimum barrel thickness decreases. In contrast to rectangular arches, the size of the masonry units and the joint friction angle significantly influences the mechanical behaviour of skewed masonry arches.

Keywords: *Discrete element method, masonry, skew arches, minimum thickness, 3DEC, structures*

***Corresponding author:** Katalin BAGI, Dept. of Structural Mechanics, Budapest University of Technology and Economics, email: kbagi@mail.bme.hu*

1. Introduction

Masonry arch bridges constitute a significant proportion of European road and rail infrastructures. Most of them are well over 100 years old and support traffic loads many times above those originally envisaged. According to Orbán (2009), there are approximately

200,000 masonry arch railway bridges in Europe. This is approximately 60% of the total bridge stock. Almost 70% of these masonry arch bridges are 100-150 years old, while 12% of them are older than 150 years. In addition, a proportion of masonry arch bridges span obstacles at an angle (or skew) other than 90 degrees. This results in the faces of the arch not being perpendicular to its abutments and its plan view being a parallelogram (**Figure 1**). Most of the masonry arches have been constructed with a small amount of skew (i.e. less than 45º), since those with large amount of skew present significant construction difficulties (Melbourne and Hodgson, 1995). Different materials and methods of construction used in these bridges will influence their strength and stiffness. Although a great deal of work has been carried out to assess the strength of square or regular masonry arch bridges (Heyman 1966; Gilbert 1993; Page 1993; Melbourne and Hodgson 1995), comparatively little work has been undertaken to understand the behaviour of skew arches (Hodgson 1996; Wang 2004; Sarhosis et al. 2014). The analysis of skew arch bridges involves many difficulties and there is no universally accepted method of analysis yet. Today, in many countries, including UK, masonry skew arch bridges routinely assessed based on the assumption that they are rectangular in shape with an equivalent span of the skewed arch bridge (e.g. BD 21/01). However, experience from current studies (Hodgson 1996; Sarhosis et al. 2016; Sarhosis et al. 2014) demonstrated that this approach leads to conservative results, which is not representative of the actual strength and stiffness of the structure. Therefore, there is an increasing demand to understand the life expectancy of such bridges in order to inform maintenance, repair and strengthening strategies.

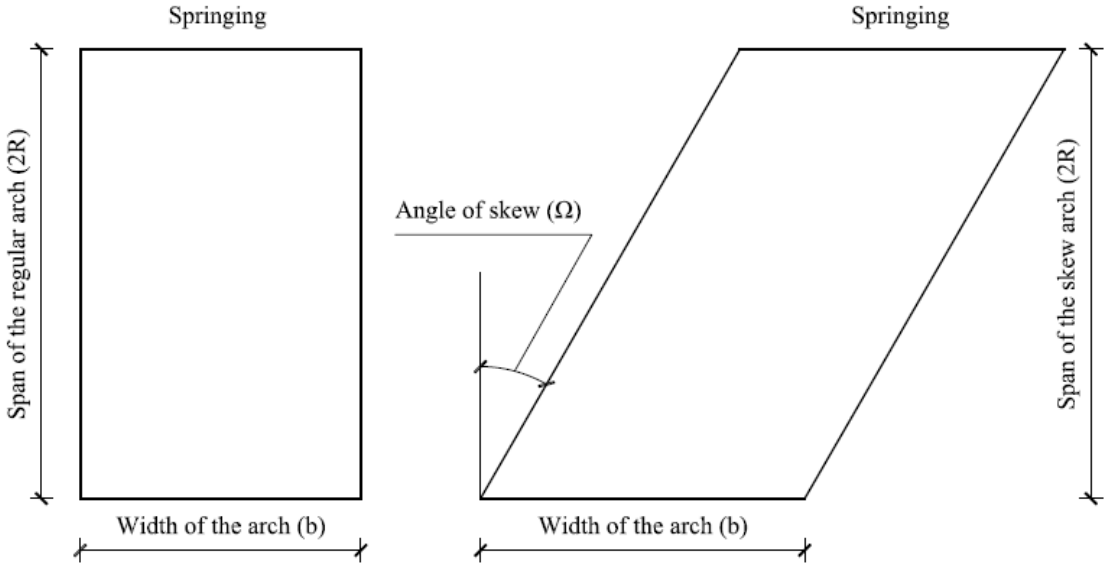

***Figure 1** – Plan view of a regular and a skew arch*
(R is the corresponding radius of the mid-surface)

In recent years, sophisticated methods of analysis, like Finite Element Method (FEM), have been applied to understand the three dimensional behaviour of arches (Choo and Gong 1995). An overview of the different models performed in the 1990's can be found in Boothby (2001) and Sarhosis et al. (2016). However, in such models, the description of the discontinuity is limited since they tend to focus on the continuity of the arch. Sophisticated FEM approaches (e.g. contact element techniques) are able to reflect the discrete nature of masonry. Examples of such models undertaken by Fanning and Boothby (2001), Gago et al. (2002), Ford et al. (2003) and Drosopoulos et al. (2006). The disadvantages of these methods are mainly

associated with: a) high computational cost; b) inability to predict realistically the crack development at serviceability limit state; and c) convergence difficulties when blocks fall or slide excessively. An alternative and appealing approach is that represented by the Distinct Element Method (DEM), where the discrete nature of the masonry arch is truly incorporated. The advantage of the DEM is that it considers the arch as a collection of separate voussoirs able to slide and rotate relative to each other. The DEM was developed by Cundall (1971) to model blocky-rock systems and sliding along rock mass. The approach was later used to model masonry structures including arches (Lemos, 1995; Lemos, 2007; Mirabella and Calvetti, 1998; Tóth et al., 2009; Sarhosis and Sheng, 2014; Sarhosis et al., 2015), where failure occurs along mortar joints. These studies demonstrated that DEM is a suitable method to perform analysis of low bond strength masonry where failure is mainly at masonry unit-to-mortar interface (Giamundo et al. 2014).

Masonry arch bridges are composed of different structural components (e.g. piers, barrel, backfill, spandrel walls, parapets and wing walls) which interact each other. However, in order to understand the behaviour of masonry arch bridges, first it is of value to study each component separately and then move on and study their interaction. In this paper, use is made of the discrete element method of analysis for the calculation of the minimum barrel thickness necessary for equilibrium of semi-circular masonry arches subjected to their own weight. In case of regular arches, the issue is settled: The purely rotational collapse mechanism that develops when the thickness of the arch is critically small have been investigated analytically and graphically by Milankovitch (1907) (see also Foce 2007) and found that forms a symmetric five-hinge mechanism just before collapse. However, up to now, no research work has been undertaken to investigate the minimum arch thickness of skew arches. Although the analysis of regular arches can be undertaken in two-dimensional space, the analysis of skew arches requires analysis in three-dimensional space. So, the three dimensional software 3DEC based on the Discrete Element Method (DEM) of analysis was used. Within DEM, each masonry unit of the arch is represented by a rigid element. Mortar joints are represented as zero thickness interface elements which can open and close according to the magnitude and direction of stresses applied to them. Also, a sensitivity study has been carried out to investigate the influence of the minimal barrel thickness with respect to the: a) angle of skew; b) construction method (e.g. false, helicoidal, and logarithmic method); c) size of masonry units; and d) frictional resistance between masonry units.

2. Constructional aspects of skewed masonry arch bridges

Masonry is strong in compression, but relatively weak in tension. Therefore, regular masonry arch bridges designed to be constantly under compression. To achieve this, the direction of forces within the arch should be normal to the coursing joints surface so that there will be no tendency in the successive courses to slide upon each other. The same idea also adopted for the construction of masonry skew arches. In the 19th century, engineers, mathematicians and masons understood that for an arch to stand, the line of pressure should be parallel to the face of the arch. Hence, they positioned the voussoirs (e.g. stones, bricks) in such a way that the coursing joint surfaces should always be perpendicular to the face of the arch at every elevation. The other important factor considered for the construction of the skew arches related to the construction difficulties. Masons realised that construction was far easier when voussoirs had exactly the same size and were rectangular cuboid in shape. From the above

observations, over the years, three main types of construction evolved for circular arches. These shown in ***Figure 2***:

a) **False skew arch:** This is the simplest form of construction where units are laid parallel to abutments (**Figure 2a**)

b) **Helicoidal method (or English method):** In this method, the coursing joints are perpendicular to the face of the arch only at the crown. The coursing joints follow helix spirals. The advantage of this method is that each voussoir is similar in shape and size to all other voussoirs. However, for geometrical reasons and for the beds to remain parallel, the orientation of the block units causes the beds to "roll over" and thus rest on the springings at an angle. Gaps between masonry units in the arch usually filled with mortar (**Figure 2b**)

c) **Logarithmic method:** In this method, the coursing joints are perpendicular to the face of the arch at all elevations. This is the most expensive method of construction since it requires varying sized masonry blocks and availability of high skilled masons, since almost every block in the arch barrel is of unique shape (**Figure 2c**)

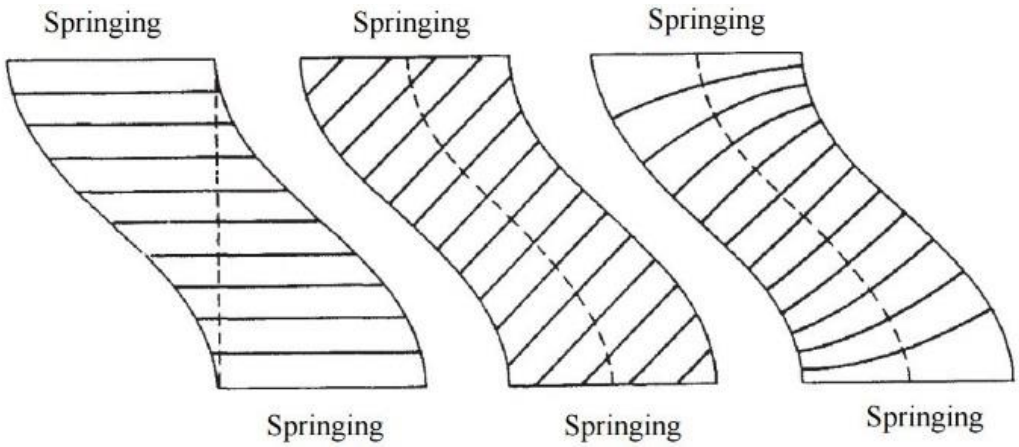

Figure 2 *– Developments and coursing joints of the different methods of construction (Melbourne and Hodgson, 1995)*

According to Rankine (1898) and Gay (1924), in general, masonry skewed arches constructed using the following three steps:

a. Construction of formwork representing the mid-surface of the skewed arch;
b. Determination of the equation of coursing and heading joints on the formwork. The position of each voussoir was marked on a sheet, which was laid down on the formwork.
c. Planar coordinates of each voussoir extruded into the 3D space.

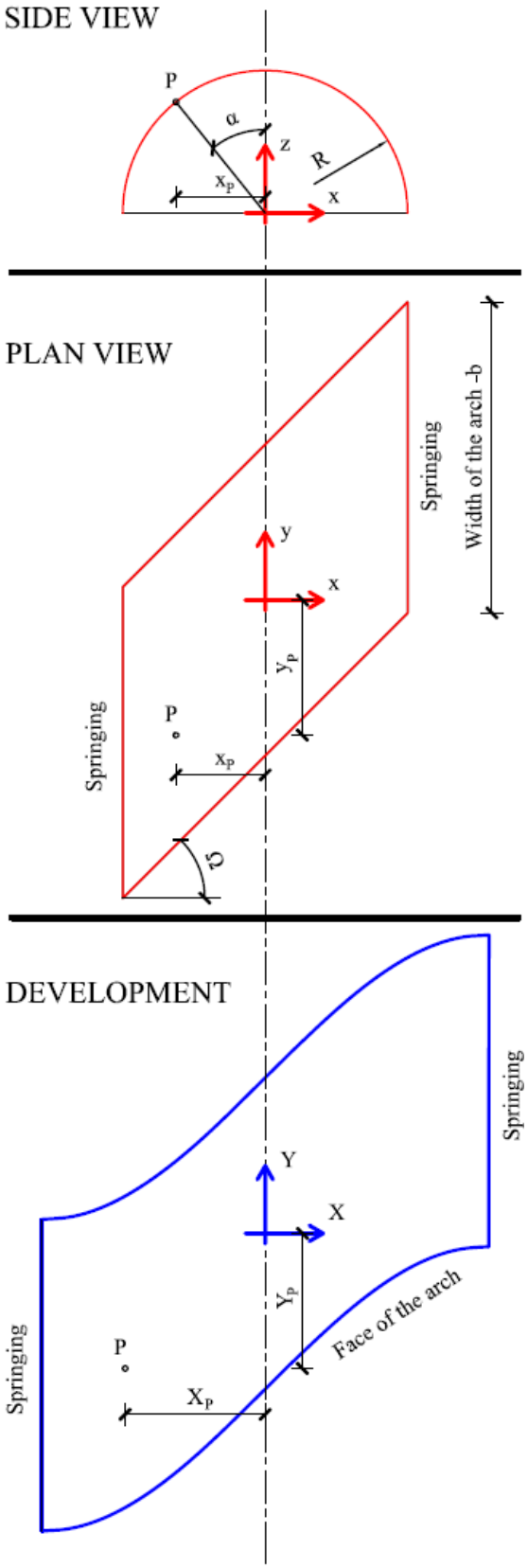

Figure 3 *– Characteristic views for a cylindrical skew arch*

2.1. Calculation of the mid-surface of a skewed masonry arch

Assume a thin, flexible and inextensible sheet that coincides with the surface of a cylinder. Then, this sheet can be extended on a plane without being rumpled or torn. With the help of the notations shown in Figure 3, the mid-surface of the skew arch is given by Equation 1:

$$Y_{face} = \frac{R}{\tan(\Omega)} \cdot \sin\left(\frac{X}{R}\right) \pm \frac{b}{2}, \qquad -R\frac{\pi}{2} \leq X \leq R\frac{\pi}{2} \tag{1}$$

where Y_{face} is the vertical coordinate of the face of the arch on the developed surface, R is the radius of the arch, Ω is the angle of skew, b is the width of the arch, and X is the horizontal coordinate on the developed mid-surface.

Also, the springing lines on the development can be written as:

$$X = \pm R\frac{\pi}{2} \tag{2}$$

2.2. Equations of coursing and heading joints for the different construction method

2.2.1. False skew arch

The geometrical construction of the false skew arch (Figure 4) is the simplest of the three methods. All of the coursing joints are parallel to the springing line. The heading joints are perpendicular to the coursing joints. Therefore, the nodes of the elements can be calculated on the cylindrical surface directly. In this method, all voussoirs have the same size and shape apart from the ones in the faces of the arch.

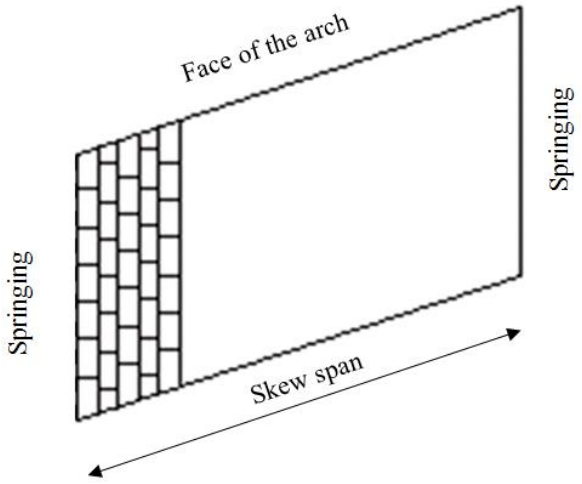

***Figure 4** – Plan view of skew arch constructed according to the false method*

2.2.2. Logarithmic method

The coursing joints of an equilibrated skew arch intersect at right angles the curve formed by the intersection of the soffit with any plane parallel to the faces of the arch. Let's assume that $Y = f(X)$ is the equation to a curve which intersects the curve of the arch's face at right angle in the point P.

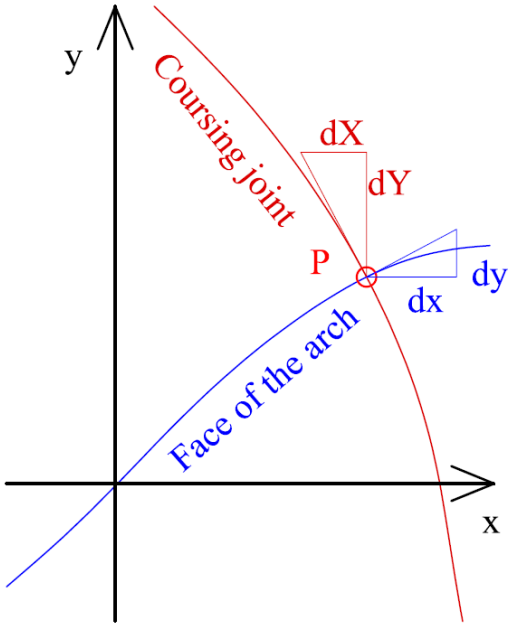

***Figure 5** – The perpendicularity condition for logarithmic method*

Then, at this point the two curves have an intersection point, and their tangent are perpendicular to each other at this point (***Figure 5***):

$$y = Y, \qquad x = X, \qquad and \qquad \frac{dy}{dx} = -\frac{dX}{dY} \tag{3}$$

The equation of the arch's face is known, so the derivative of it can be calculated:

$$\frac{cos\left(\frac{x}{R}\right)}{\tan(\Omega)} = -\frac{dX}{dY} \tag{4}$$

Integrating the above formula with respect to x:

$$Y(X) = -\int \frac{\tan(\Omega)}{cos\left(\frac{X}{R}\right)} dX = -\frac{R}{\tan(\Omega)} \cdot \ln\left(sec\left(\frac{X}{R}\right) + tan\left(\frac{X}{R}\right)\right) + c_{1i} \tag{5}$$

The c_{1i} constant in the equation of i^{th} coursing joint should be determined in that way that the distance between the adjacent coursing joints should be equal at the centreline of the arch. To determine these c_{1i}constants the arc length of the centreline should be calculated. The curve of the centreline is equivalent with the curve of the arch's face, which is a sinusoidal curve in the development and it is equivalent with a semi-ellipse in the 3D-space. The procedure to calculate the arch length of an arbitrary curve is presented below (see ***Figure 6***). Let's assume:

$$\Delta s = \sqrt{\Delta x^2 + \Delta y^2} = \sqrt{1 + \left(\frac{\Delta y}{\Delta x}\right)^2} \cdot \Delta x \tag{6}$$

Let's take the limit of Δs as Δx approaches zero:

$$\lim_{\Delta x \to 0} \Delta s = \sqrt{1 + \left(\frac{dy}{dx}\right)^2}\, dx \tag{7}$$

Let's integrate the above function to obtain the length of the centreline of the arch:

$$\int_{\frac{-R\pi}{2}}^{\frac{R\pi}{2}} ds = \int_{\frac{-R\pi}{2}}^{\frac{R\pi}{2}} \sqrt{1 + \left(\frac{dy}{dx}\right)^2}\, dx \tag{8}$$

In case of the arch' face this expression leads to a complete elliptic second order integral:

$$s = \int_{\frac{-R\pi}{2}}^{\frac{R\pi}{2}} \sqrt{1 + \frac{1}{tan^2(\Omega)}} \sqrt{1 - \frac{1}{tan^2(\Omega) + 1}\left(\sin\left(\frac{x}{R}\right)\right)^2}\, dx \tag{9}$$

Also, the arc length was split into *n* equal parts according to the number of courses.

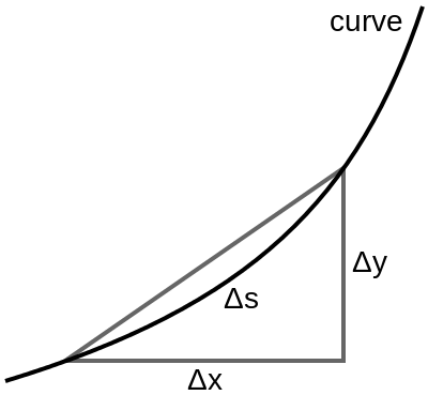

Figure 6 *– Arc length of an arbitrary curve*

Using equation 10, x_i can be determined.

$$\int_{\frac{-R\pi}{2}}^{x_i} \sqrt{1 - \left(\frac{dy_{face}}{dx}\right)^2}\, dx - s\frac{i}{n} = 0 \tag{10}$$

Finally, the c_{1i} constants can be obtained from:

$$c_{1i} = y_{face}(x = x_i) - y_{coursing_{joint_i}}(x = x_i) \tag{11}$$

The curves of the heading joints are parallel to the face of the arch:

$$Y_{heading\_joint\_j} = R_{mid} \cdot \tan(\Omega) \cdot \sin\left(\frac{X}{R_{mid}}\right) + c_{2j} \qquad -\frac{b}{2} \leq c_{2j} \leq \frac{b}{2} \tag{12}$$

The c_{2j} constants should be equally spaced between the two face of the arch depending on how many elements should be in one course. The coursing joints follow logarithmic curves, while the heading joints are parallel to the face of the arch. The intersection point of the heading and coursing joints is representing the vertex of the element. At this point a bisection-method was implemented to solve these equations. (Newton-method would have convergence problems). Then, the coordinates were transformed back to the intradosal and extradosal cylindrical surface by the following transformation:

$$x_{int} = \mathrm{R}_{int} \sin\left(\frac{X}{R_{mid}}\right) \qquad and \qquad x_{ext} = \mathrm{R}_{ext} \sin\left(\frac{X}{R_{mid}}\right) \tag{13}$$

$$y_{int} = Y \qquad and \qquad y_{ext} = Y \tag{14}$$

$$z_{int} = \mathrm{R}_{int} \cos\left(\frac{X}{R_{mid}}\right) \qquad and \qquad z_{ext} = \mathrm{R}_{ext} \cos\left(\frac{X}{R_{mid}}\right) \tag{15}$$

2.2.3. Helicoidal method

In case of helicoidal method the coursing joints are helix spirals. These spirals appear as straight lines on the developed surface. This idea was described firstly by Nicholson (Nicholson, 1828) to describe the surface of the intrados by using the simplifications that the arch barrel consists of a single ring having a relatively small thickness. Later, the idea of Nicholson expanded by Fox (Fox, 1836), where he considered the intrados of the barrel and the extrados as separate surfaces mapped onto concentric cylinders by drawing a separate development for each surface. In this way, a third theoretical surface can be developed, which is an intermediate surface located at the mid-way between the intrados and the extrados. The mid-surface of the arch allowed the masons to align the centre of each voussoir, rather than its inner surface, along the desired line.

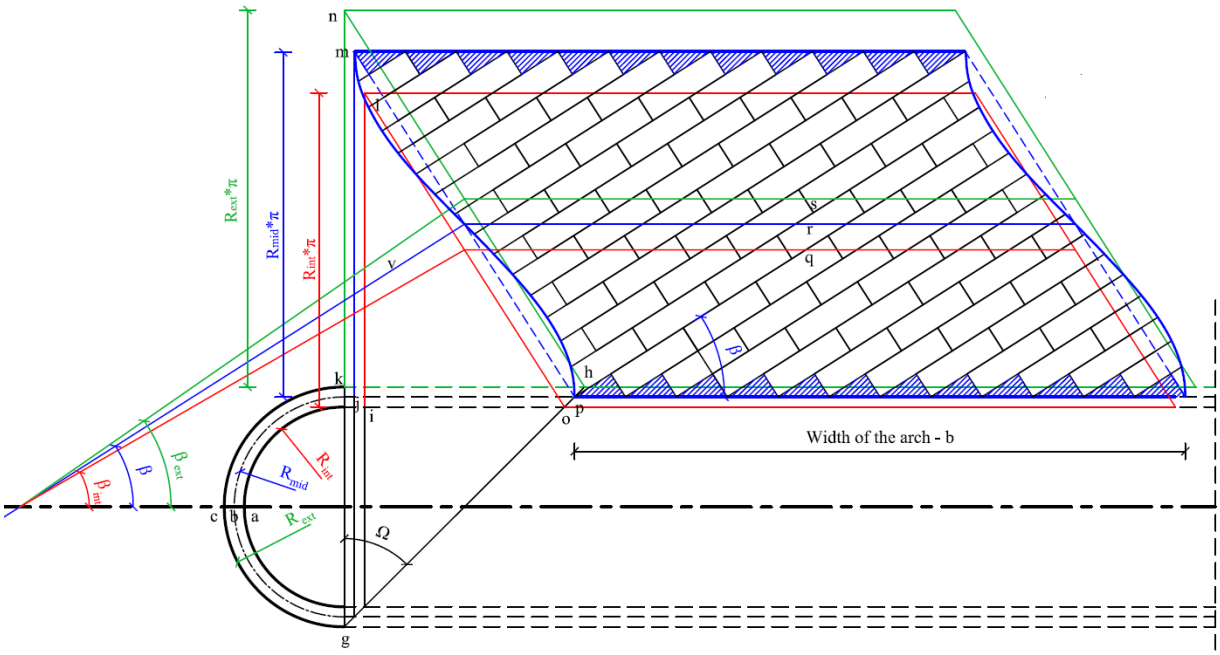

Figure 7 *– Charles Fox's drawing type design method to construct the developed surfaces.*

In order to visualize the courses of voussoirs in a stone skew arch, Fox wrote, "The principle which I have adopted is, to work the stones in the form of a spiral quadrilateral solid, wrapped round a cylinder, or, in plainer language, the principle of a square threaded screw". Hence, the transverse sections of all the spiral stones are the same throughout the whole arch. It will be obvious, that the beds of the stones should be worked into true spiral (helicoidal) planes. So, a stone skew arch built to Fox's plan would have its voussoirs cut with a slight twist, in order to follow the shape of a square threaded screw.

From ***Figure 7***, on the developed extradosal and intradosal surfaces the coursing joints are not parallel with the coursing joints of the mid-surface. In this way, β, β_{ext} and β_{int} can be computed from equations 16 and 17.

$$\beta = \arctan\left(\frac{2 \cdot R_{mid} \cdot \tan(\Omega)}{R_{mid} \cdot \pi}\right) = \arctan\left(\frac{2 \cdot \tan(\Omega)}{\pi}\right) \tag{16}$$

$$\beta_{int} = \arctan\left(\frac{R_{int} \cdot \tan(\beta)}{R_{mid}}\right), \quad \beta_{ext} = \arctan\left(\frac{R_{ext} \cdot \tan(\beta)}{R_{mid}}\right) \tag{17}$$

3. Overview of modelling masonry arches with 3DEC

Within discrete element method, masonry is represented as an assembly of rigid or deformable blocks. 3DEC is a commercial code released by ITASCA CG. A 3DEC model consists a set of polyhedral bodies. Joints are viewed as the surfaces where mechanical interaction between blocks takes place, governed by appropriate constitutive laws. The motion of the blocks is simulated throughout a series of small but finite time-steps, numerically integrating the Newtonian equations of motion.

3.1 Masonry units

In 3DEC, the polyhedralblocks may be convex, or concave blocks can be created by joining single convex blocks. They may even contain holes. The masonry units can be represented as perfectly rigid or deformable blocks. In the present study, masonry units assumed as rigid bodies with six degrees of freedom (three translational and three rotational).

3.2 Representation of contacts

To check all possible pairs of elements for contact, the search time increases quadratically with the number of the blocks. To avoid it, in 3DEC before a pair of blocks can be checked for contact using exact geometrical calculations by the computer program, candidate pairs are identified first (Cundall, 1988).

In this first step an envelope space is assigned to every block as the smallest three-dimensional box with sides parallel to the coordinate axes that can contain the block. Those pairs of blocks are then tested for contact in detail whose envelope spaces intersect.

After two blocks have been recognized as neighbours, then they are tested for contact. Contact created when a point of a block gets into the interior of another block. The contact detection algorithm recognizes these situations, and also provides a unit normal vector, which defines the plane along which sliding can occur. This unit normal should change direction continuously as the two blocks move relative to each other.

Similar to other DEM codes with polyhedral elements, 3DEC applies a scheme based on a *"common plane between the two blocks"*. The contact detection analysis consists of the following two parts:

- Determine a "common-plane" that, roughly saying, bisects the space between the two blocks;
- Test both blocks separately for contact with the common-plane.

The common plane is defined as the resulting plane provided by the optimization problem "*Maximize the gap between the common plane and the closest vertex"* or, equivalently, "*Minimize the overlap between the common-plane and the vertex with the greatest overlap*". The algorithm applies a gradual translation and rotation of the common plane in order to maximize the gap (or minimize the overlap).

Contact exists if the overlap is positive, or equivalently, if the gap is negative between the two blocks. The normal vector of the common plane is the contact normal. When a face of a rigid block is in contact with the common plane, then it is automatically discretized into sub-contacts by triangulating the face. The vortices of the triangles will be the nodes whose translation increments during the actual time-step serve as the basis for the calculation of the forces transmitted between the two contacting blocks.

The area "owned" by each sub-contact is, in general, equal to one-third of the area of the surrounding triangles around the node. This calculation is adjusted when the sub-contact is close to one or more edges on the opposing block. If the other side of the interface is also a face, then identical conditions apply: sub-contacts are created, and relative displacements, and hence forces, are calculated. Details of special cases like e.g. edge-to-edge contacts are not presented here for simplicity.

The basis of the mechanical calculations is the relative velocity of the sub-contact under question. This is defined as the velocity of the analysed node minus the velocity of the corresponding point of the opposite face on the other block. This latter velocity can be calculated with the help of a linear interpolation of the three nodes on the surface of the other block surrounding that opposite point. Then the relative translation vector belonging to the sub-contact is calculated from the relative velocity and from the length of the time step. This relative translation is multiplied with the actual normal and shear stiffness of the contact, in order to receive the uniform distributed normal and shear forces belonging to the sub-contact. The resultant along the sub-contact area is assigned to the analysed node; and the opposite of the resultant is shared among the three nodes surrounding the coincident point on the opposite face. The same is done for all nodes on the analysed face of the first block. Then the other block is analysed in a similar manner: Nodes along its contacting face are considered, and another set of sub-contacts is produced where the sub-contact forces are calculated from the corresponding relative displacements.

Consequently, when two blocks come together, the contact logic described above is equivalent to two sets of sub-contacts in parallel, each carrying sub-contact forces. The sub-contact forces received in the two steps are summed and halved then, in order to receive the overall interface behaviour as the average of that of both sets.

3.3 Constitutive models for contacts

The mechanical behaviour of contacts in 3DEC is modelled with the help of contact stiffness defined in the normal and shear directions, relating sub-contact stresses with relative displacements characterizing the sub-contact.

According to e.g. Lemos (2007) the normal stiffness in 3DEC can have different physical interpretations even in those cases when the blocks are deformable. In the case of mortared joints, the normal stiffness can be directly related to mortar thickness and its physical properties. For dry joints, rough and irregular contact surfaces have a finite stiffness against penetration, which is reflected by the contact normal stiffness. In the shear direction, shear stiffness plays a similar role and Coulomb friction sets a limit to the sub-contact shear stress magnitude. In case of perfectly rigid blocks in the 3DEC model, on the other hand, the contact stiffness data have to represent the block deformability as well; Simon and Bagi (2016) provide a short analysis how to relate the contact stiffness parameters to the mechanical data of the contacting voussoirs.

Though finite tensile strength and a joint dilatation angle could also be included in 3DEC. In the elastic range (when contact sliding and separation does not occur) the behaviour is governed by the joint normal and shear stiffness (k_n and k_s):

$$\Delta F^n = -k_n \cdot \Delta U^n \cdot A_c \quad (18)$$

$$\Delta F^s = -k_s \cdot \Delta U^s \cdot A_c, \quad (19)$$

where $\Delta F^n, \Delta F^s$is the normal and the shear force increment (resultant for the sub-contact); k_n, k_s are the joint normal and the joint shear stiffness; ΔU^n, ΔU^s are the normal and the shear displacement increments belonging to the sub-contact; and A_c is the sub-contact area.

The maximum shear force allowed is given by:

$$F^s_{max} = F^n \cdot \tan(\varphi), \tag{20}$$

where φ the angle of friction.

3.4 Equations of motion for rigid blocks

The equations of translational motion for a single block can be expressed as

$$\ddot{x}_i + \alpha \dot{x}_i = \frac{F_i}{m} + g_i, \tag{21}$$

where $\ddot{x}_i$ is the acceleration of the centroid of the block; $\dot{x}_i$ the velocity of the centroid of the block; α is the viscous (mass-proportional) damping constant; F_i is the sum of forces acting on the block (contact + applied external forces, except gravitational forces); m is the mass of the block; and g_i is the gravity acceleration vector.

The rotational motion of an undamped rigid body can be most efficiently described if referred to the principal axes of inertia of the body. However, blocks in 3DEC are oriented typically in random directions compared to the global coordinate axes of the system. Because velocities are small, the rotational equations can be simplified. Accurate representation of the inertia tensor is not essential. Therefore, in 3DEC only an approximate moment of inertia is calculated, based upon the average distance from the centroid of vertices of the block. This allows the rotational equations to be referred to the global axes. The angular acceleration (ω_i) about the principal axis can be calculated by equation 22:

$$\dot{\omega}_i + \alpha \omega_i = \frac{M_i}{I}, \tag{22}$$

where α is the viscous (mass-proportional) damping constant; M_i is total torque; and I is the approximate moment of inertia. For quasi-static analysis, isotropic inertia tensor is only used in 3DEC. For dynamic problems, the real inertia tensor is required. Time integration of the equations of motion is done with the central finite difference scheme. The velocities and angular velocities are calculated as follows:

$$\dot{x}_i\left(t + \frac{\Delta t}{2}\right) = \left[\left(1 - \alpha\frac{\Delta t}{2}\right) \cdot \dot{x}_i\left(t - \frac{\Delta t}{2}\right) + \left(\frac{F_i(t)}{m} + g_i\right) \cdot \Delta t\right] \cdot \frac{1}{1 + \alpha\frac{\Delta t}{2}} \tag{23}$$

$$\omega_i\left(t + \frac{\Delta t}{2}\right) = \left[\left(1 - \alpha\frac{\Delta t}{2}\right) \cdot \omega_i\left(t - \frac{\Delta t}{2}\right) + \left(\frac{M_i(t)}{I} + g_i\right) \cdot \Delta t\right] \cdot \frac{1}{1 + \alpha\frac{\Delta t}{2}} \tag{24}$$

The increments of translation and rotation are given by

$$\Delta x_i = \dot{x}_i\left(t + \frac{\Delta t}{2}\right) \cdot \Delta t \tag{25}$$

$$\Delta \theta_i = \omega_i\left(t + \frac{\Delta t}{2}\right) \cdot \Delta t \tag{26}$$

The position of the block centroid is updated as:

$$x_i(t + \Delta t) = x_i(t) + \Delta x_i \tag{27}$$

The location of the vertices is calculated with the help of the displacement of the centroid plus the rotation calculated earlier.

3.5 Mechanical damping

Damping is applied in 3DEC to decrease false oscillations originating from the explicit nature of the time integration technique, and to facilitate to reach a force equilibrium state as quickly as possible. Damping has to fulfill two different (and partly contradicting) roles in a 3DEC simulation at the same time: (1) it has to represent the physically existing energy dissipation in the system; and (2) it has to ensure numerical stability and fast convergence. Two forms of damping can be applied in 3DEC. The first one is named "*adaptive global damping*", in which viscous damping forces are used, but the viscosity constant is continuously adjusted in such a way that the power dissipated by damping is a given proportion of the rate of change of kinetic energy in the system. This suggested proportion is 50% (ITASCA, 2004), chosen according to exhaustive numerical experimenting by the developers of 3DEC.

In the second form named "*local damping*", different damping force and moment components are applied on every degree of freedom. Every component is proportional to the magnitude of the unbalanced force or moment. For this scheme, referred to as "local damping", the direction of the damping force is always opposite to the actual translational or rotational velocity.

If the system tends to an equilibrium state (e.g. to a state with constant velocities), local damping gradually disappears, and becomes zero in the equilibrium state. The adaptive global damping is efficient when the system oscillates around the equilibrium state (ITASCA 2004). Preliminary experiences gained on test examples showed that shorter computational time was needed to find the equilibrium state when adaptive global damping was used, so in the static analysis in the present paper adaptive global damping was used. A convergence test has also been performed and it was found that the results were not affected for values of damping different from 0.5. So the default value 0.5 has been used in the present investigations.

3.6 Numerical stability

The central difference method is only conditionally stable. To avoid numerical instabilities, a limiting timestep is defined in 3DEC and the user is allowed only to decrease it. In case of rigid elements, the limiting timestep is calculated by analogy to a simple degree-of-freedom system, as:

$$\Delta t_b = frac \cdot 2 \cdot \left(\frac{M_{min}}{K_{max}}\right)^{0.5}, \tag{28}$$

where M_{min} is the mass of the smallest block in the system; K_{max} is the maximum contact stiffness; $frac$ is a user-defined value that accounts for the fact that a block may be in contact with several neighbouring blocks. The simulations in the present paper were done with the default value, *frac* = 0.1.

4. Computational modelling of skewed masonry arches

4.1. Development of the arch geometry

Geometric models representing skewed masonry arches constructed using different construction methods have been generated. Since only polyhedral elements with planar faces can be generated in 3DEC, for the construction of even slightly concave elements, adjacent convex polyhedral blocks were generated and joined together. The variation of geometrical characteristics for the arches used in the computational analysis is shown in **Table 1.**

Table 1. *– Variation of the geometrical characteristics for the arches used in the computational analysis.*

Radius of the arch (m)	Width of the arch (m)	Angle of skew (degrees)	Length-to-width ratio of the voussoirs	Block width (m)
3.00	5.00	0; 15; 30; 45	0.5; 1; 1.5; 2; 3; 4; 5	0.250

4.1.1 False skew arch

For the construction of the geometry of the false skew arches, blocks generated in a stretcher bond pattern by assigning a predefined off-set to every second course. The construction process for a false skew arch is shown in ***Figure 8***. Initially, a wide regular arch has been constructed (***Figure 8a***). The arch was then intersected by two vertical skew planes defining the angle of skew (***Figure 8b***), leaving an irregular end finish which later "corrected" by adding adjacent blocks (***Figure 8c***). Typical geometries of false skew arches with different angles of skew are shown in ***Figure 9***.

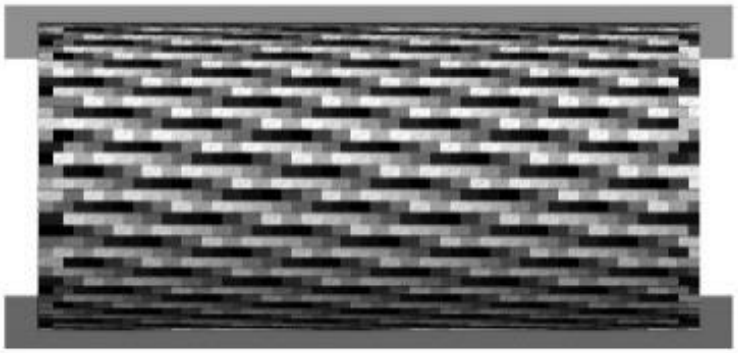

(a)

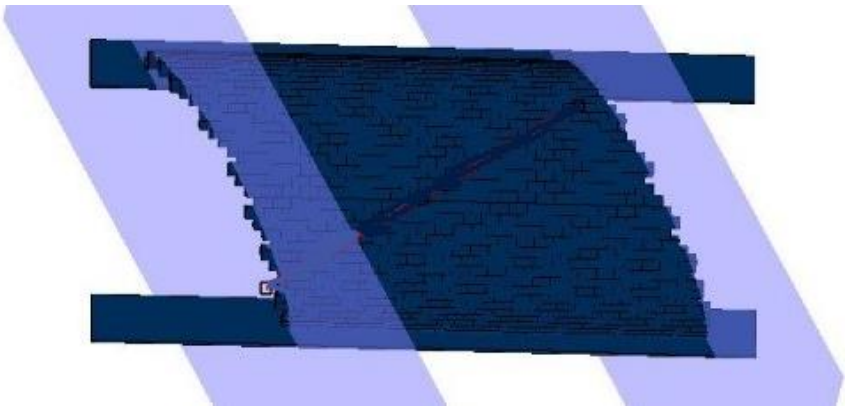

(b)

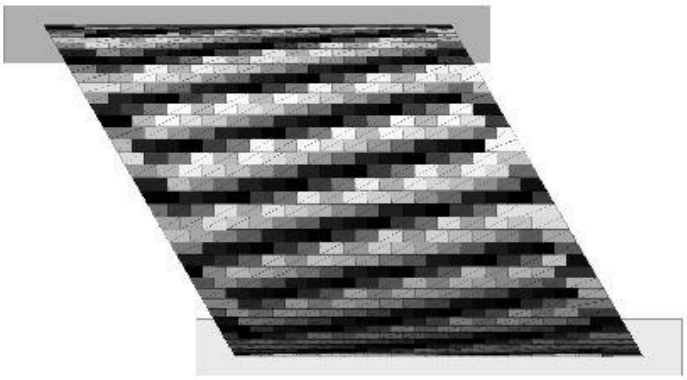

(c)

Figure 8 *– Development of a false skew arch from a regular arch*

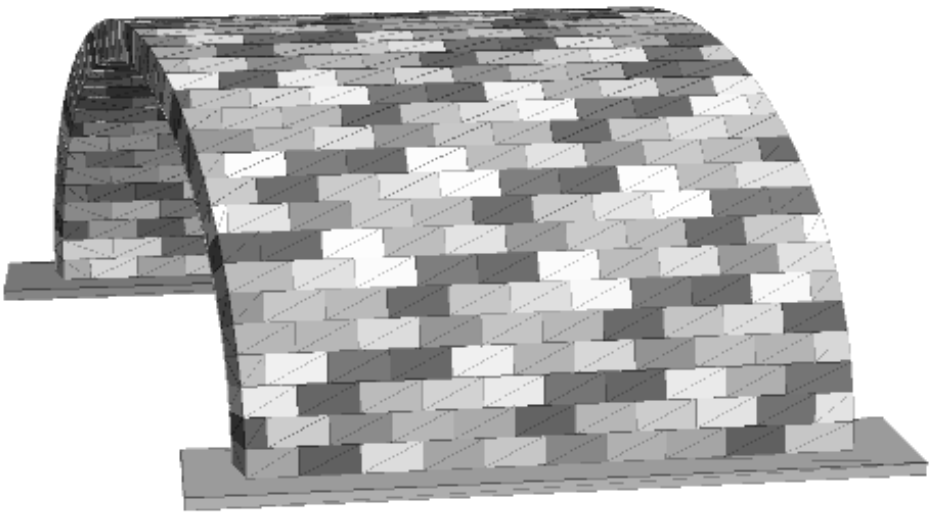

(a) Angle of skew is 15°

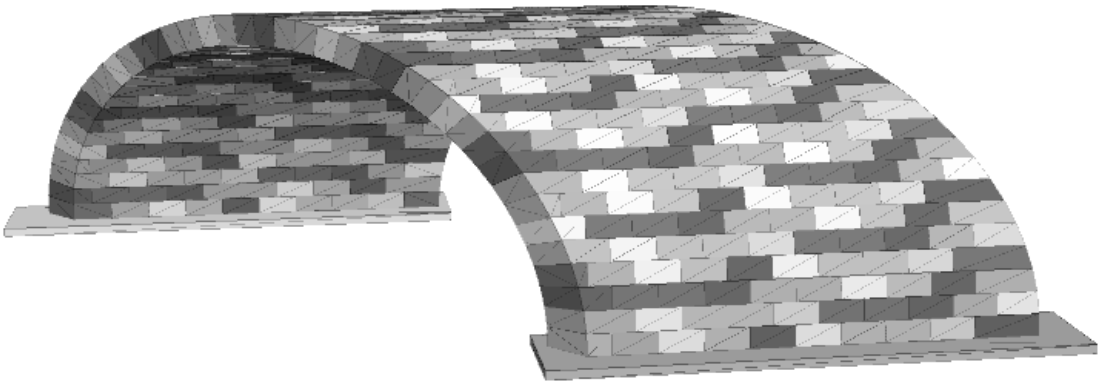

(b) Angle of skew is 45°

***Figure 9**– Geometrical models of skewed masonry arches constructed using the false method*

4.1.2 Helicoidal method

For the generation of the skewed masonry arches using the helicoidal method, the edges of the masonry units were not straight and the faces were not planar. The voussoirs were divided into tetrahedral parts, which joined together to form the masonry unit blocks. For the construction of the helicoidal method, three types of masonry units are generated (***Figure 10***). These are:

- **Support units**: These elements connect the abutments with the voussoirs.
- **Regular units:** These form the majority of the masonry units and are identical in shape and size.
- **Quoins:** These masonry units represent the face of the arch.

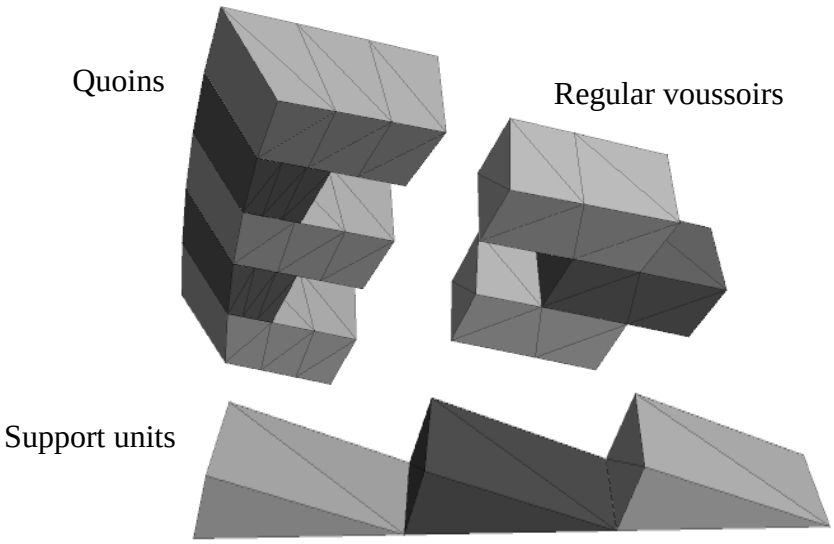

Figure 10 *– Elements of the helicoidal skew arch: quoins (top left), normal units (top right), support elements (bottom)*

Typical geometries of skew arches using the helicoidal method with different angles of skew are shown in ***Figure 11***.

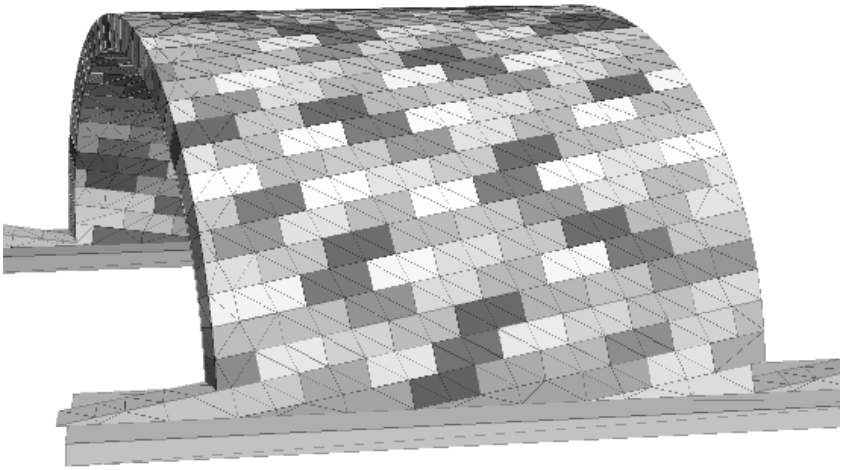

(a) Angle of skew is 15°

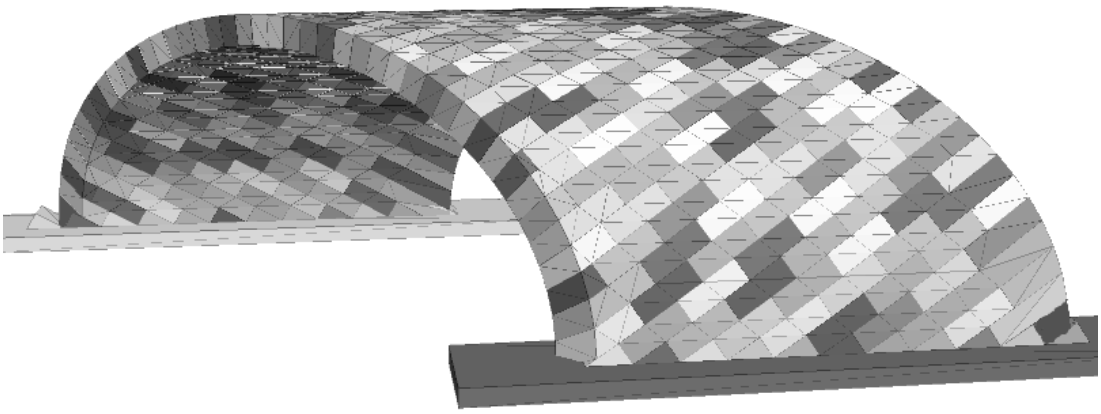

(b) Angle of skew is 45°

Figure 11 *– Geometrical models of skewed masonry arches constructed using the helicoidal method*

4.1.3 Logarithmic method

For masonry skewed arches constructed with the logarithmic method, the faces of any of the voussoirs in the arch are not planar. During construction of skew masonry arches based on the logarithmic method, mortar is filled between the arches to overcome this geometrical difficulty. However, in 3DEC only polyhedral bodies can be generated with planar faces (mortar represented as zero thickness interface). Hence, voussoirs were split into tetrahedrons and joined together. Also, adjacent courses were generated such that they ran in a stretcher bond. ***Figure 12*** shows masonry arches with different skew angles constructed using the logarithmic method. As the angle of skew increases, the unit width at the acute angle also increases while the width of the unit at the obtuse angle decreases.

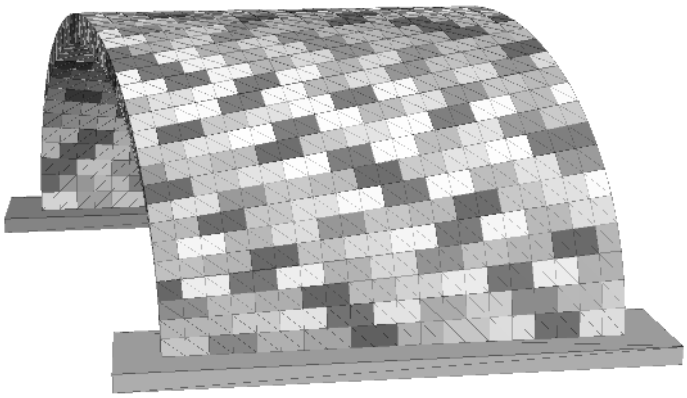

(a) Angle of skew is 15°

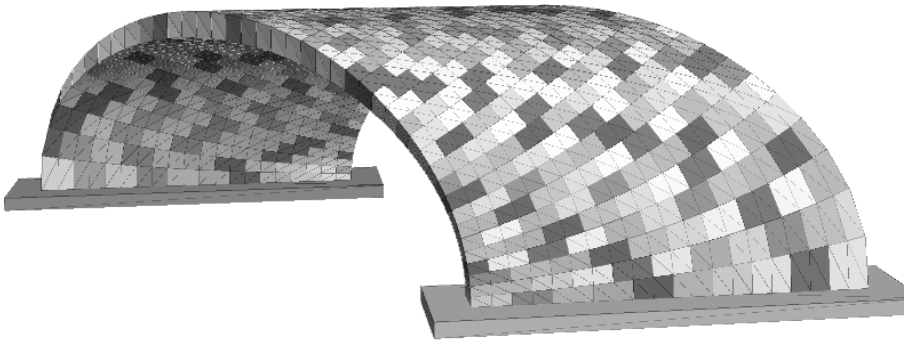

(b) Angle of skew is 45°

Figure 12 *– Geometrical models of skewed masonry arches constructed using the logarithmic method*

5. Material parameters and boundary conditions

Each masonry unit of the arch is represented by a rigid block separated by zero thickness interface at each joint. The density of each block was equal to 2,700 kg/m^3 (Sarhosis et al. 2014). However, from a sensitivity study carried out by Sarhosis et al (2014), it was found that the critical barrel thickness does not depend on the density of the blocks. The zero thickness interface between adjacent blocks has been modelled using the elastic perfectly plastic Coulomb-slip failure criterion, endowed with a tension cut-off. The joint interface contact parameters obtained from Jiang and Esaki (2002) are shown in ***Table 2.*** Joint tensile strength, cohesive strength and dilation angle assumed zero. However, frictional resistance between masonry units has been allowed. Since the intention of the authors was to investigate the effect of the arch ring geometry, the abutments of the arch were modelled as rigid supports

in the vertical and horizontal directions. Self-weight effects were assigned as gravitational load. Gravitational forces give rise to compressive forces within the blocks of the arch and result in the stabilisation of the arch. The model brought into equilibrium under its own self-weight and displacements at the intrados of the arch have been recorded. The model was considered to be in equilibrium when the maximum out-of-balance force was less than 0.001% of the total weight of the structure. Failure considered when the maximal displacement exceeded 0.2m.

Table 2. *Properties of the joint interface for the development of the computational models*

Joint Normal Stiffness (N/m^3)	**Joint Shear Stiffness (N/m^3)**	**Joint Friction (degrees)**	**Joint Dilatation Angle (degrees)**
7.64×10^9	1.79×10^9	40°	0°

6. Verification study

6.1. Rotational failure mode

The problem of identifying the minimum thickness of regular (e.g. zero skew) circular masonry arches when subjected to self-weight have been investigated by several researchers (Ochsendorf (2002), Heyman (1966), Alexakis and Makris (2013)). From these studies, the minimum thickness and location of the imminent intrados hinge identified. Couplet (1730) based on observations noted that for a full semi-circular arch, the angular position of the haunches' hinges (β_{cr}) is at 45° from the vertical axis and the minimum thickness t_{min} is equal to $0.101\times R$, where R is the distance from the centre of circle to the mid-surface thickness of the arch. Two centuries later, Heyman (1977) using analytical formulations found that for a semi-circular arch, β_{cr} is equal to 58.82° and t_{min} is equal to $0.105965 \times R$. However, as described by Cocchetti et al. (2011), Heyman's work has been based on under-conservative assumptions, including: a) the true location of centre of gravity of each ideal voussoir of the arch is not on the centre-line of the arch; and b) the position of thrust line at the intrados hinges is tangential to the intrados. A more accurate approach derived from Milankovitch (1907), found that β_{cr} is equal to 54.48° and t_{min} is equal to $0.107478 \times R$ (Alexakis and Makris 2013; Ochsendorf 2002). In the present study, the numerical results obtained using DEM found to be very close to the theoretical solution of Milankovitch (***Figure 13***). From ***Figure 13***, the precision of the developed DEM model is ± 1.5° and $\pm\ 0.0005 \times R$. The relatively small difference in results arises from a) the discrete element model consists of discrete blocks, while Milankovitch's derivations assumed a homogenous material where cracks can develop anywhere along the arch; b) in the discrete element model the equations of motion are written always on the current geometry, which means that the changes in shape caused by the selfweight are taken into account.

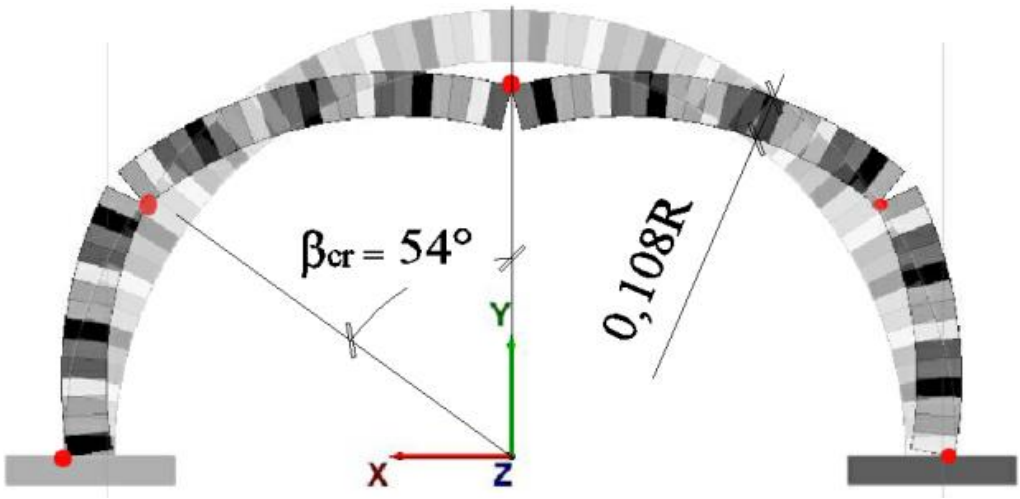

Figure 13 – Angular position of the haunches' hinges β_{cr}, and critical barrel thickness obtained from the developed numerical model based on DEM

6.2. Necessary angle of friction

The DEM model also verified by investigating the sliding type of failure. Sliding failure occurs when the thrust-force reaches the boundary of the cone of friction ($\alpha = \varphi$) (***Figure 14***). The angle has been formed using the thrust-force and the contact normal determines the necessary angle of friction to avoid sliding type of failure.

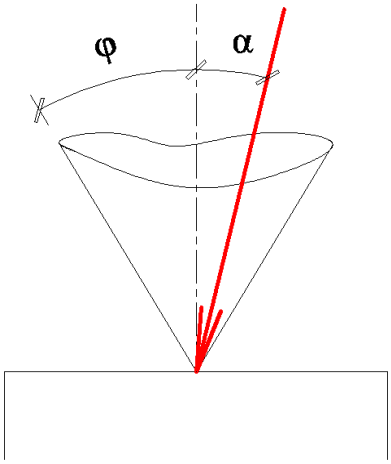

Figure 14 *– Cone of friction*

A rectangular arch with radial joints was built in the computational model where the barrel thickness was equal to the critical barrel thickness. The minimum thickness of a regular arch is the thickness that will bring the arch at the verge of becoming a five-hinge mechanism. Therefore, the thrust-line will pass by the imminent hinge of the arch at the extrados point at the crown (O_2) and at the springing (O_1) (Makris and Alexakis (2013). The horizontal force (H) at the crown has been determined from the moment equilibrium written to O_1 (***Figure 15***).

$$\sum M_i^{(O_1)} : -W\left(R + \frac{t}{2} - x_c\right) + H\left(R + \frac{t}{2}\right) = 0 \tag{29}$$

The direction of the thrust-force at a given β angle has been determined as arctan(W_β/H), where W_β is the weight of the slice according to ***Figure 15b***.

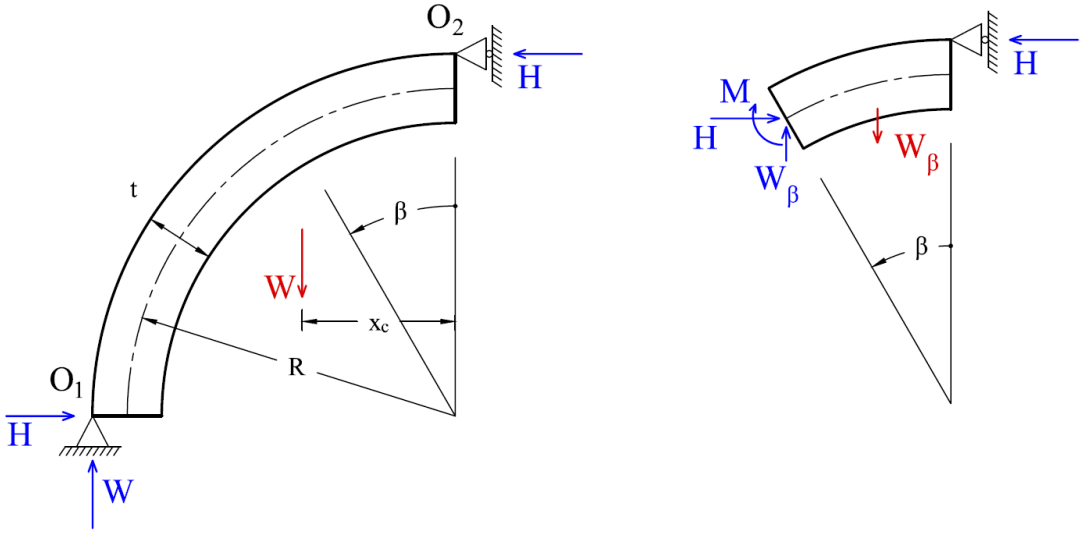

(a) *(b)*

Figure 15 *- Circular arch with radial joints at the verge of collapse*

The necessary angle of friction as a function of β angle is shown in ***Figure 16.*** The maximal frictional resistance should exist at the springing line of the arch, where $\beta=\pi/2$. The analytically observed minimum necessary angle of friction that prevents shear sliding is equal to 21.57°. In the developed discrete element model, a shear sliding failure mechanism observed when friction angle was 21°. In the case that the friction angle increases to 22°, the arch is standing.

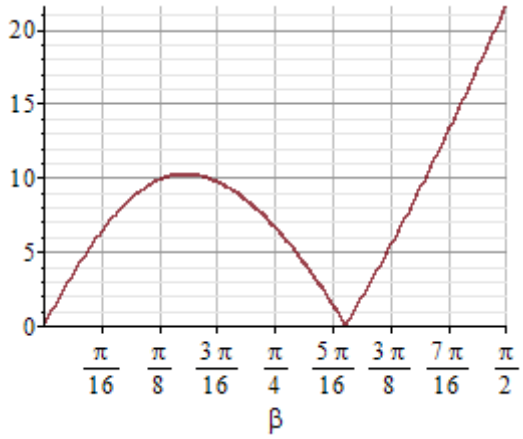

Figure 16 *– The necessary angle of friction*

7. Results and discussion

A sensitivity study carried out to investigate the variation of the minimum (or critical) barrel thickness of an arch with respect to:

a) The construction method (e.g. false, logarithmic, helicoidal)
b) The angle of skew;
c) The size and shape of the masonry units; and
d) The joint friction angle between adjacent masonry units.

During the calculation of the minimum thickness of the arch, the resolution was $\pm 0.0005R$ and increments of $0.001R$ were used; where R is the radius of the barrel (see ***Figure 3***).

7.1 Influence of the construction method on the minimum thickness of skewed masonry arches

Twelve different in geometry computational models have been created using 3DEC. **Table 3** shows the geometrical properties of the arches used in the analysis. For all arches, the joint friction angle kept constant and equal to 40 degrees. The angle of skew varied from 0° (regular arch) to 45° and the length to width ratio of the masonry was kept constant ($L/W = 2$).

Table 3 *– Geometric properties of the arches used in the analysis*

Radius of the arch (m)	Width of the arch (m)	Angle of skew (degrees)	Length-to-width ratio of the masonry units	Width of the masonry unit (m)
3.00	5.00	0; 15; 30; 45	2.00	0.250

Figure 17 shows the critical barrel thickness over radius (t/R) for each of the studied arches. From ***Figure 17***, for the false skew arch, as the angle of skew increases from 0 to 45 degrees, the minimum thickness required to sustain the self-weight of the arch increases. However, for arches constructed using the logarithmic and the helicoidal method, as the angle of skew increases from 0 to 45 degrees, the minimum thickness required to sustain the self-weight of the arch decreases. The reason for the difference in results between the different construction methods is mainly due to their failure mechanism. For the false skew arch, the application of the self-weight induces a five hinge mechanism. The developed hinge lines are straight and parallel to the abutments (***Figure 18***). Similar results are also reported by Sarhosis et al. (2014). However, the failure mechanism of the helicoidal and logarithmic method differs to that of the false skew arch. In case of helicoidal and logarithmic method, hinges developed in a zig-zag pattern parallel to the abutments of the arches. This was mainly due to the arrangement of the voussoirs in the arch (***Figure 19*** and ***Figure 20***). The zig-zag hinge pattern development increases the frictional resistance and shear sliding at the hinge locations.

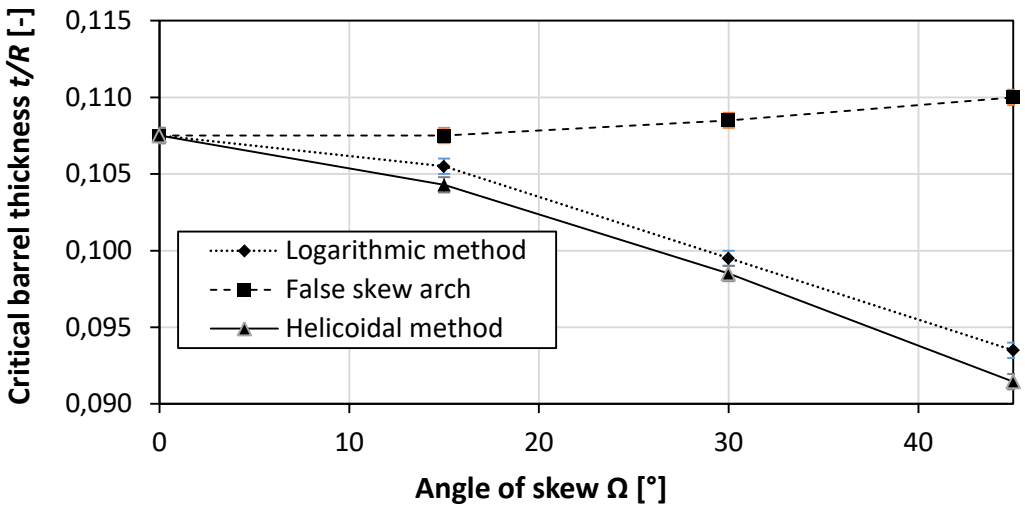

Figure 17. *– Influence of the angle of skew on the critical barrel thickness*

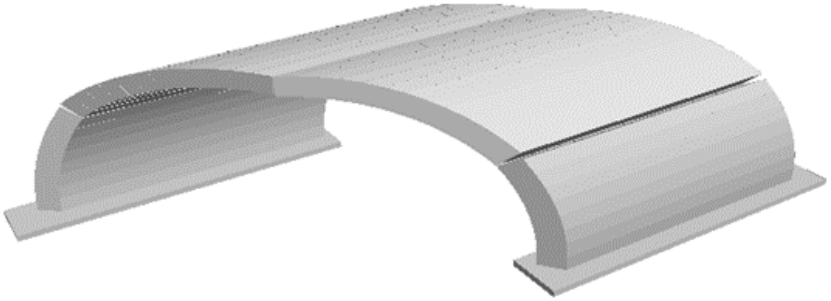

(a)

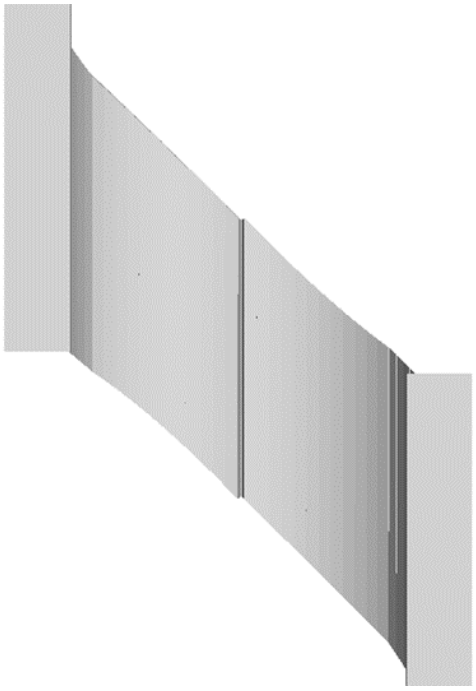

(b)

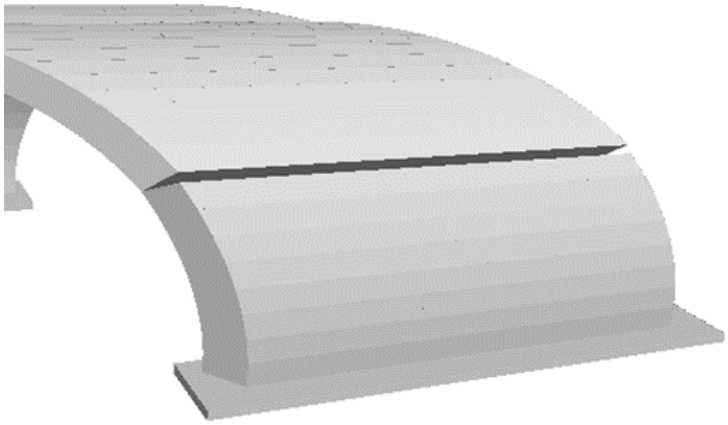

(c)

Figure 18. *– Failure mode of false skew arch (angle of skew 45°)*

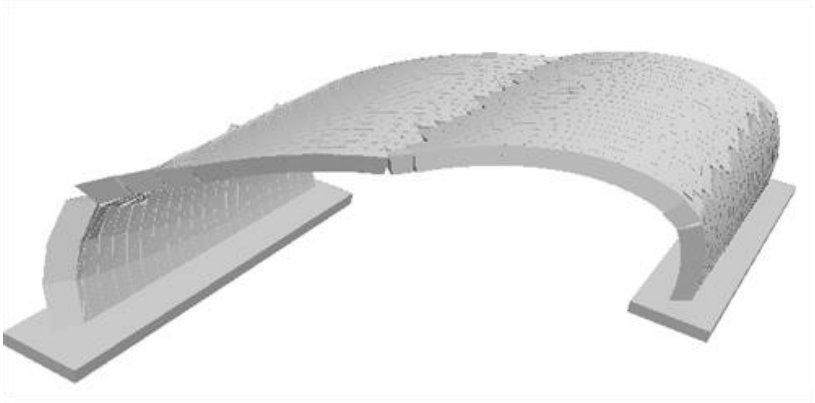

(a)

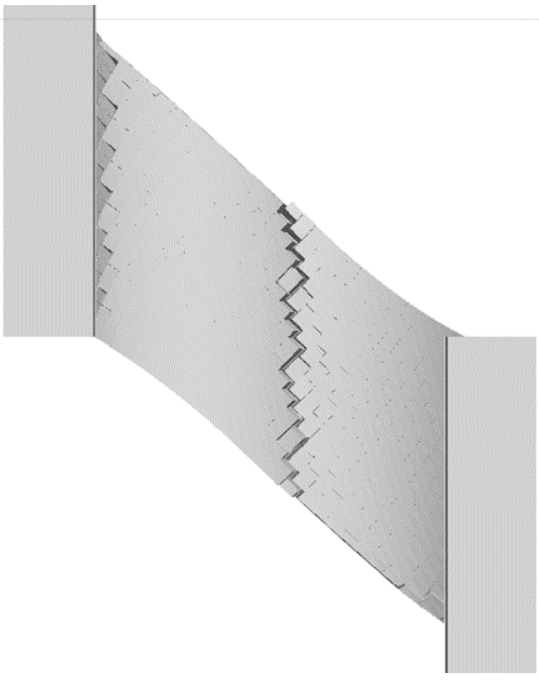

(b)

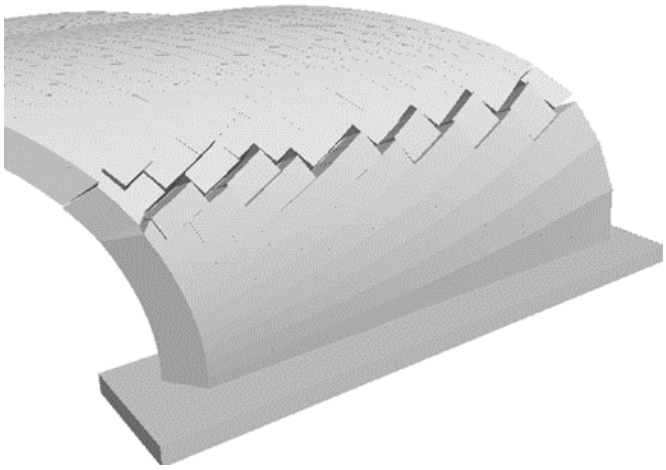

(c)

Figure 19. *- Failure mode of logarithmic masonry skew arch (angle of skew 45°)*

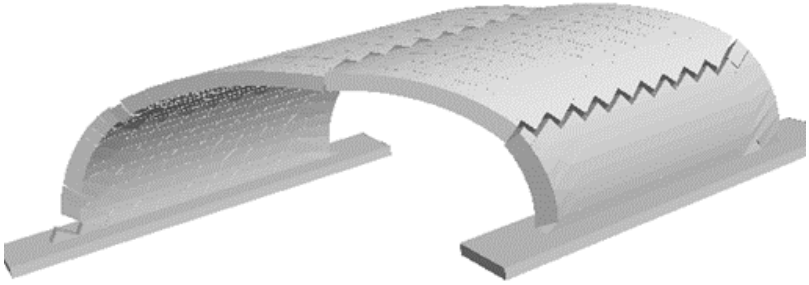

(a)

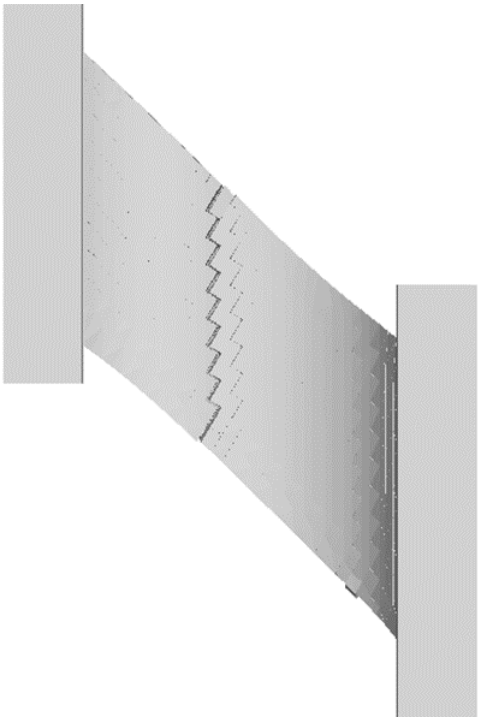

(b)

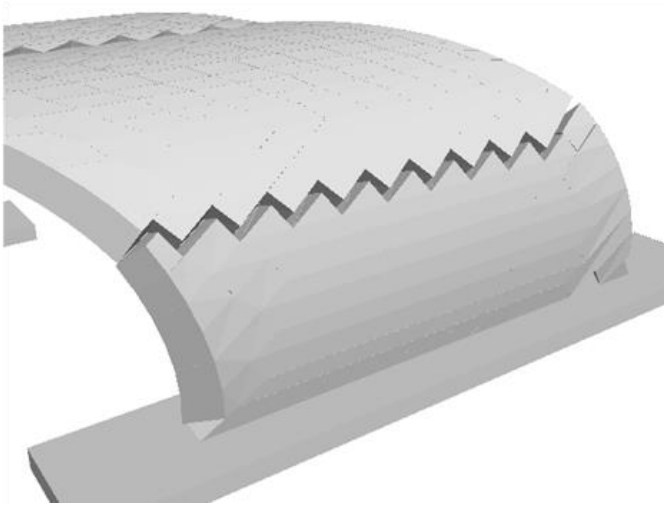

(c)

Figure 20 – *Failure mode of a helicoidal skew arch (angle of skew 45°)*

7.2 Influence of the masonry unit size on the critical barrel thickness of the arch

A sensitivity study has been undertaken to investigate the influence of the size of the masonry unit on the critical barrel thickness and failure mode of masonry skewed arches. The length (L) to width (W) ratio of masonry units ranged from 0.5 to 5 while the height of the masonry units assumed equal to the arch thickness (***Figure 21***). The geometric parameters for the different arches considered in the computational analysis are shown in **Table 1.** The joint friction angle kept constant and equal to 40°.

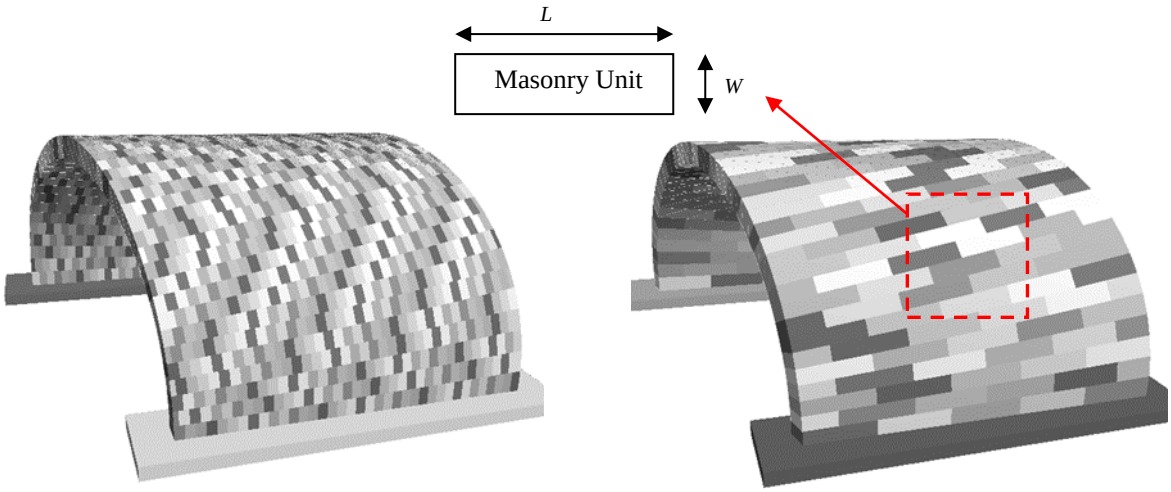

(a) Masonry unit length to width ratio equal to 1:2

(b) Masonry unit length to width ratio equal to 5:1

***Figure 21 – 5** Different element shapes (logarithmic method)*

Figure 22 shows the effect of the shape of masonry unit (L/W) to the minimum thickness over the radius of the arch (t/R) for semi-circular masonry skewed arches constructed using the false method. From ***Figure 22***, the length to width ratio of a masonry unit should be greater than the tan(Ω), for equilibrium of masonry skewed arches constructed using the false method and subjected to their own weight:

$$\frac{L}{W} \geq \tan(\Omega), \tag{30}$$

where Ω is the angle of skew. From ***Figure 22*** and for false skew arches, as the length to width ratio of masonry units increases, the critical barrel thickness tends to be equal to the critical barrel thickness of a regular arch.

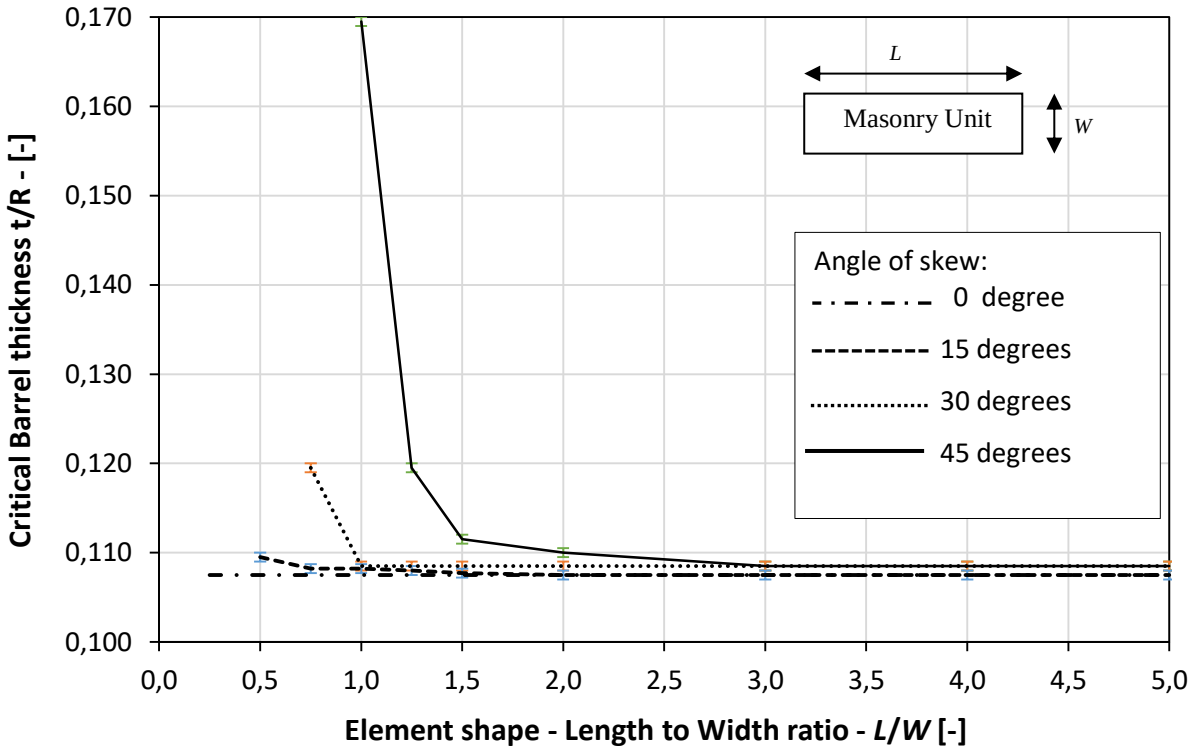

Figure 22. *– Effect of element shape – False skew arch*

In addition, it was also observed that the failure mode will differ depending on the size of the masonry units (***Figure 23***). Assuming that the compression trajectories are parallel to the face of the arch, then a moment develops which leads to cracking at the face of the arch (***Figure 24***).

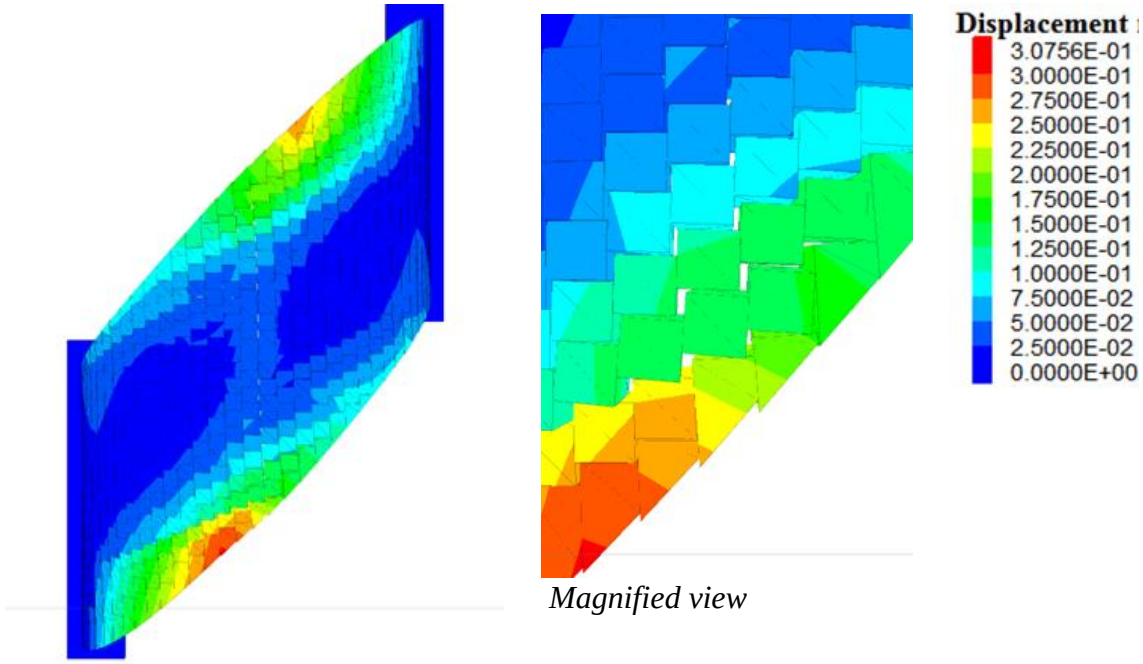

Figure 23 *– Failure mode of false skew arch in case of short element length*

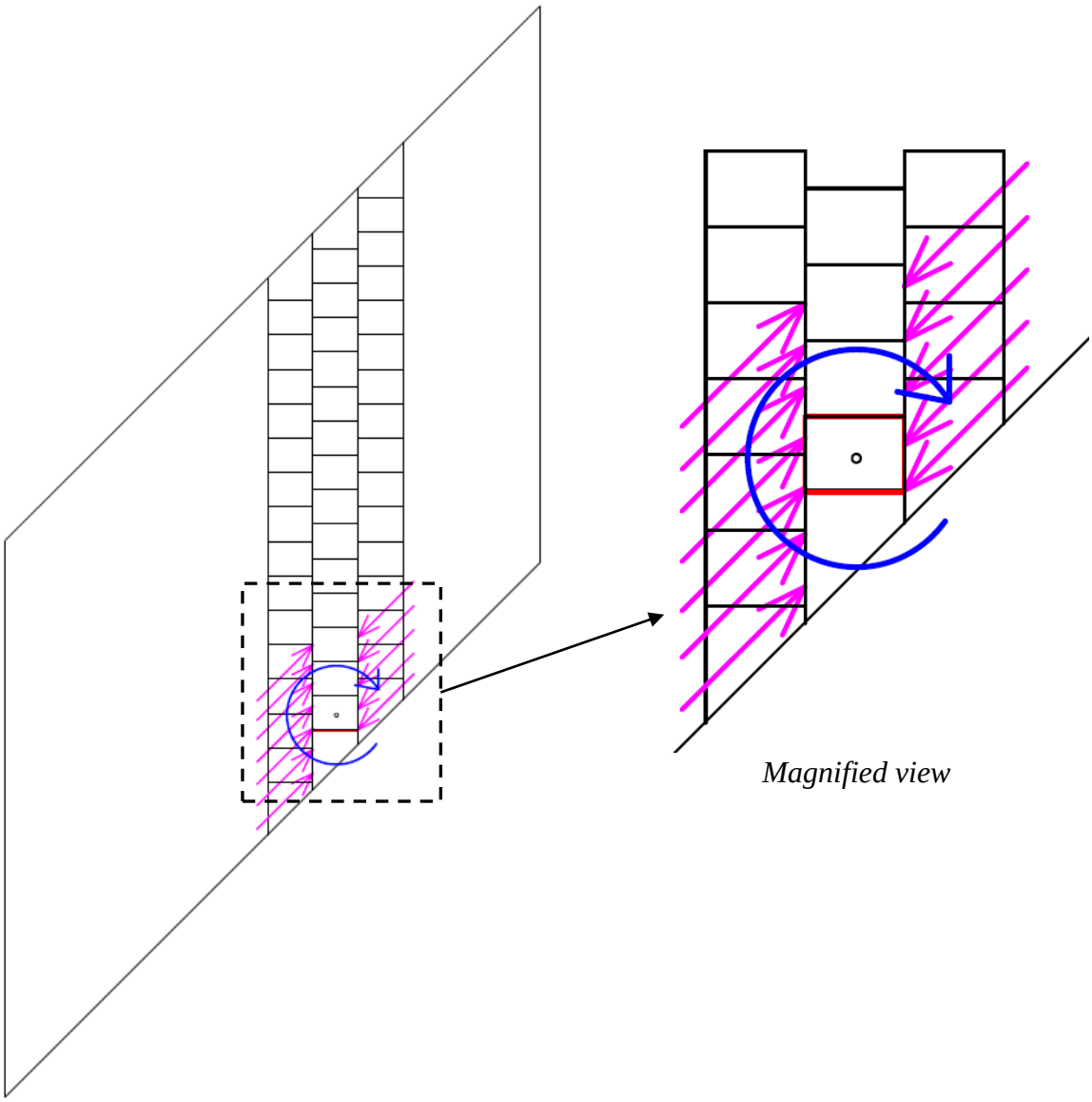

Figure 24 *– Moment arising from the skew force system*

From ***Figures*** **25 and 26** for the arches constructed using the helicoidal and logarithmic method, as the length of the masonry units increases, the critical barrel thickness linearly decreases. The failure mechanism for the masonry skew arches constructed according to helicoidal and logarithmic method influences significantly the critical barrel thickness. For masonry units with high *L*/*W* ratios, the hinges develop in zig-zag shape and neighbouring masonry units have to slide upon each other, overcoming the shear resistance in these contacts. Therefore, a lower barrel thickness compared to the false skew arch is required for the arch to stand under its self-weight **(*Figures* 19 and 20)**.

In case of helicoidal method, there was no possibility to create arbitrary element length-to-width ratio because of the restrictions made during the creation of geometry. Specific *L*/*W* ratios could be analysed only.

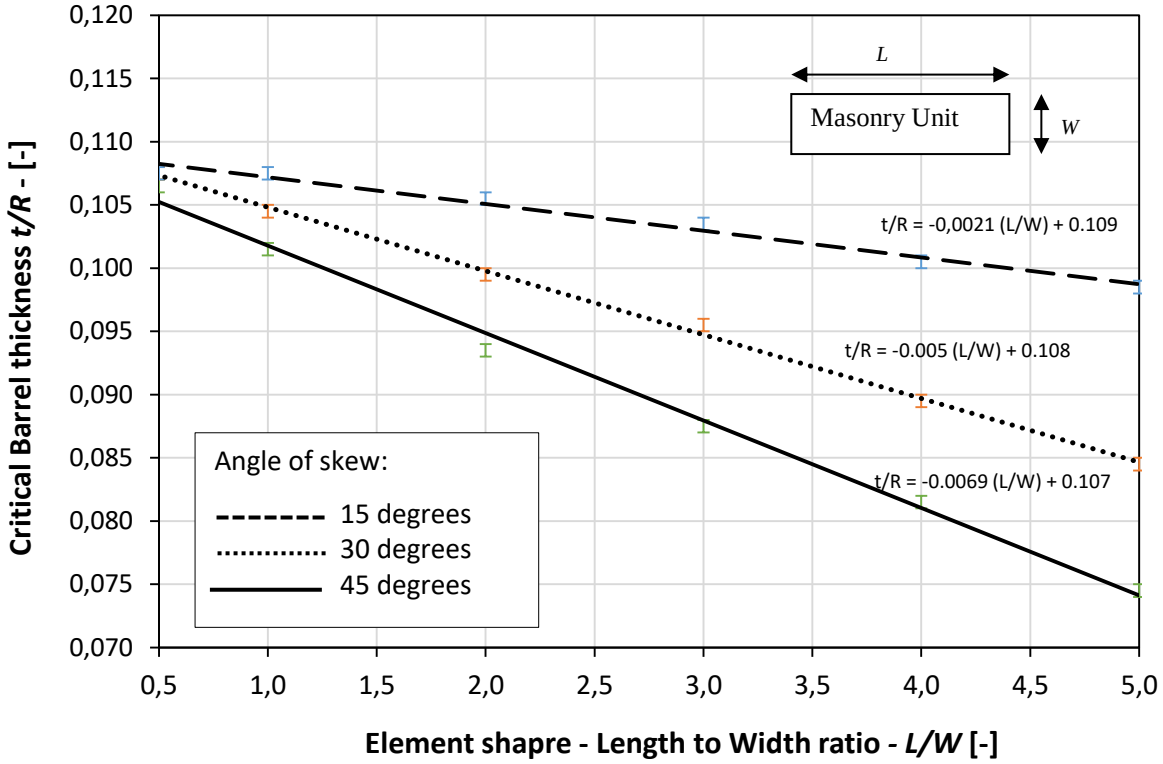

Figure 25 *– Effect of element shape – Logarithmic method*

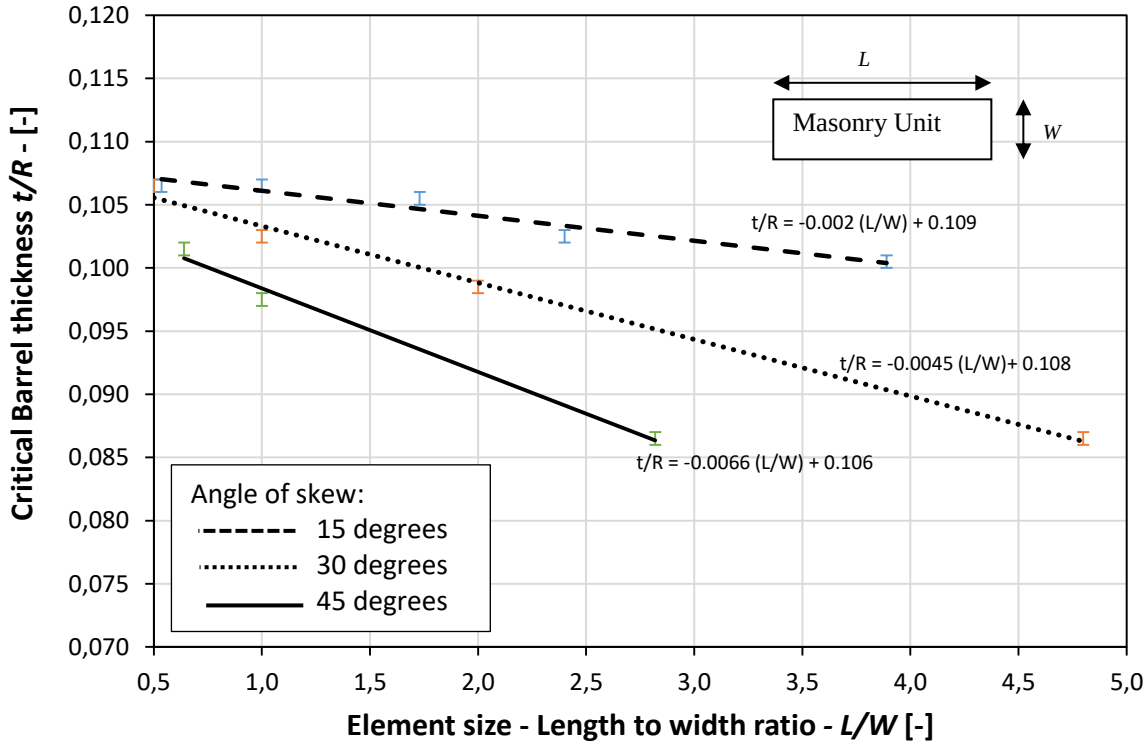

Figure 26*– Effect of element shape – Helicoidal method*

7.3 Influence of joint friction angle on the minimum barrel thickness of skewed masonry arches

A sensitivity study carried out and the joint friction angle varied from 20 to 90 degrees. Although joint friction angles greater than 60 degrees are not realistic, such analyses carried out to investigate the effect of infinite frictional resistance between masonry units. The geometric parameters for the different arches considered in the computational analysis are shown in **Table 4.**

Table 4 *- Geometrical parameters of the arches used in the analysis*

Radius of the arch (m)	Width of the arch (m)	Angle of skew (degrees)	Length-to-width ratio of the masonry unit	Width of the masonry unit (m)
3.00	5.00	45°	2:1	0.250

Figure 27 shows the effect of joint friction for 45° angle of skew. From ***Figure 26***, the critical barrel thickness decreases, as the joint friction angle increases. Also, the joint friction angle required to avoid sliding failure for a 45 degrees masonry skew arch constructed using the false method is 32.5 degrees. For values of angle of joint friction lower than 32.5 degrees, the arch collapses irrespective of the thickness of the barrel. So, the permissible joint friction angle for the arch to stand is much higher than the permissible joint friction angle for a regular arch (i.e. equal to 22 degrees) to avoid sliding type of failure (***Figure 16***). Furthermore, from ***Figure 27*** and for a false skew arch, the critical barrel thickness is constant when the angle of friction is higher than 40°. Also, ***Figure 28 Figure 28***shows the failure mode of false skew arch in case of joint friction angle smaller than 32.5°. From ***Figure 28***, the masonry units at the face of the arch slide out, which leads to the collapse of the arch.

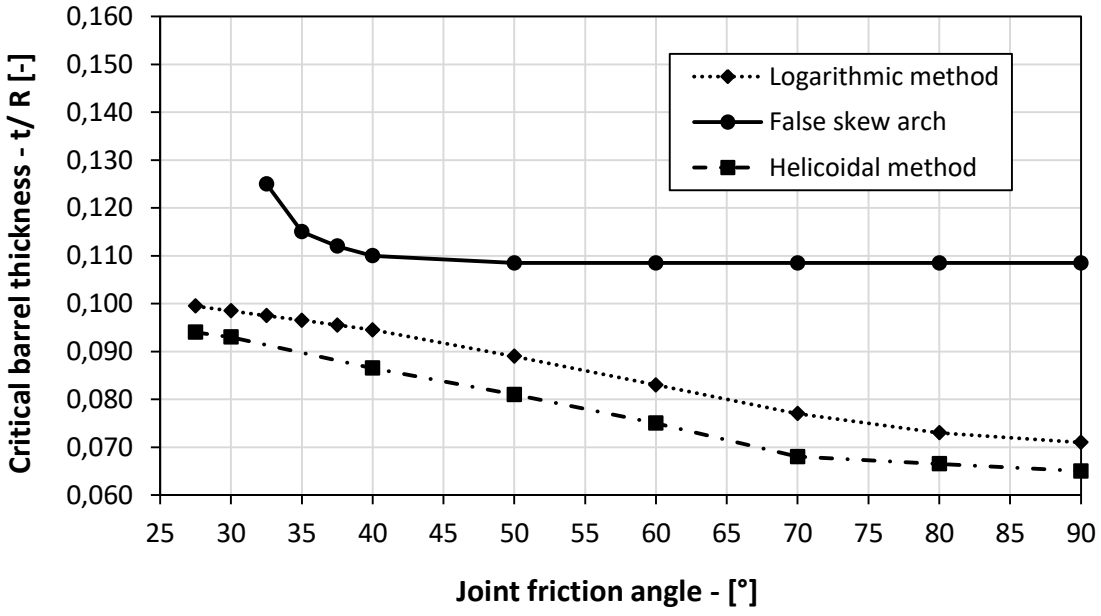

Figure 27*– Effect of joint friction for 45° angle of skew*

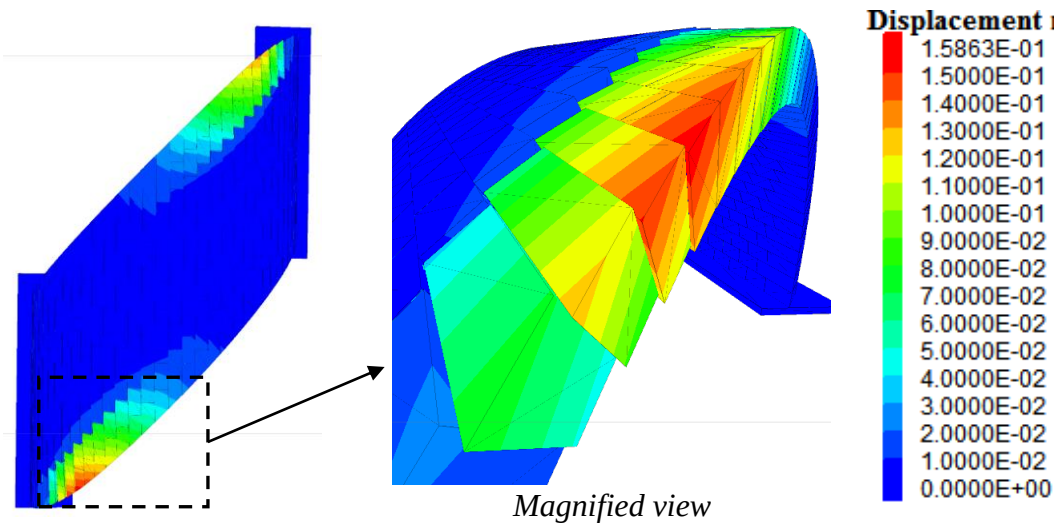

Figure 28 *– Failure mode of false skew arch in case of friction angle smaller than 32.5°*

For masonry skewed arches (45° angle of skew) constructed using the helicoidal and logarithmic method, the critical friction angle to avoid sliding is 27.5 degrees (***Figure 27***). Also, the critical barrel thickness decreases with an increase of the frictional resistance. From ***Figures 19*** and ***20***, for skew arches constructed using the helicoidal and logarithmic method, hinges develop in a zig-zag shape. Also, at the location of the hinge, adjacent masonry units slide upon each other. Since resistance against sliding increases with higher angle of friction, the critical barrel thickness to resist the self-weight of the arch will also decrease. For masonry skew arches constructed using the false method, the developed hinge lines are straight and parallel to the abutments. Hinge develops due to pure rotation of masonry units and there is no sliding or shear failure. Therefore, the critical barrel thickness is independent of the joint friction angle. ***Figures 29***, ***30 and 31*** show the ratio of shear to normal stress distribution at the joints for different in geometry masonry skewed arches. The joint friction angle for all arches kept constant and equal to 40°. The red domains represent joints where sliding resistance is nearly reached (arc tan(0.839) ≈ 40.0°). From ***Figure 29*** and for the masonry skewed arches constructed using the false method, there are two main regions where high frictional resistance is required to avoid shear sliding. These are: a) around the abutments at the obtuse angle; and b) around the unsupported part above the acute angle of the arch. The arrangement of the voussoirs is exactly alike in case of helicoidal and logarithmic method at the neighbourhood of the crown. The difference in the arrangements of the masonry units between the two methods is at the area close to the abutments of the arch. At this point the ratio of the shear versus normal contact stresses is high (***Figure 30***). This phenomenon was already known in the 19th century in the book of Hyde (1899). This is why the full-centered (***Figure 3***: opening angle: $\alpha = 90°$) helicoidal skew arch was avoided. The logarithmic method shows no tendency to slide around the abutments (***Figure 31***), but in case of high angle of skew, there is relatively high friction utilization around the imminent hinge location at the intrados.

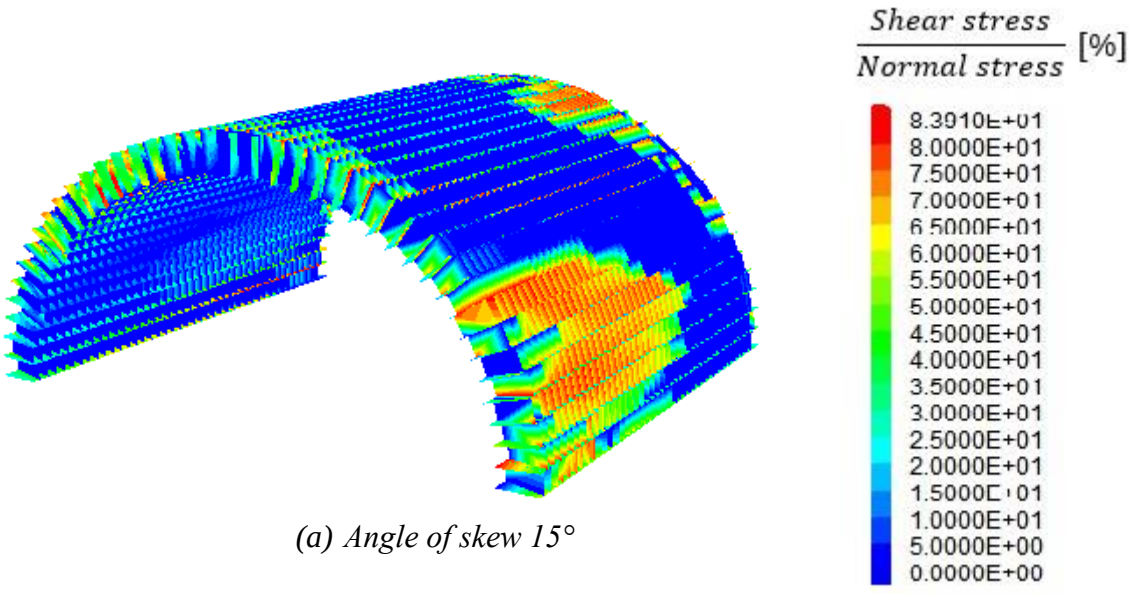

(a) Angle of skew 15°

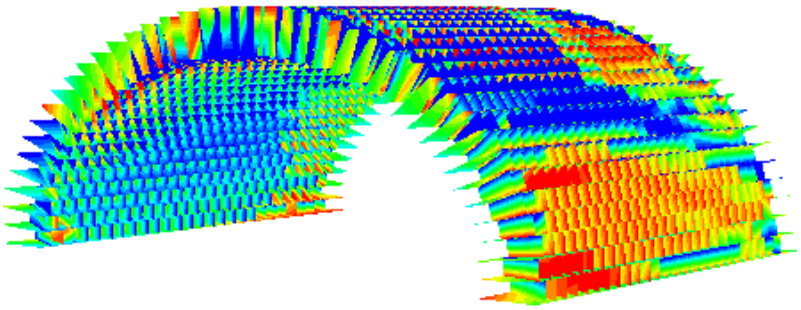

(b) Angle of skew 30°

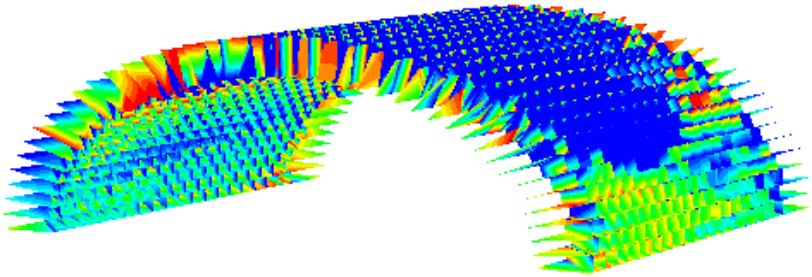

(c) Angle of skew 45°

Figure 29 *– Shear / normal subcontact stress in case of false skew arch*

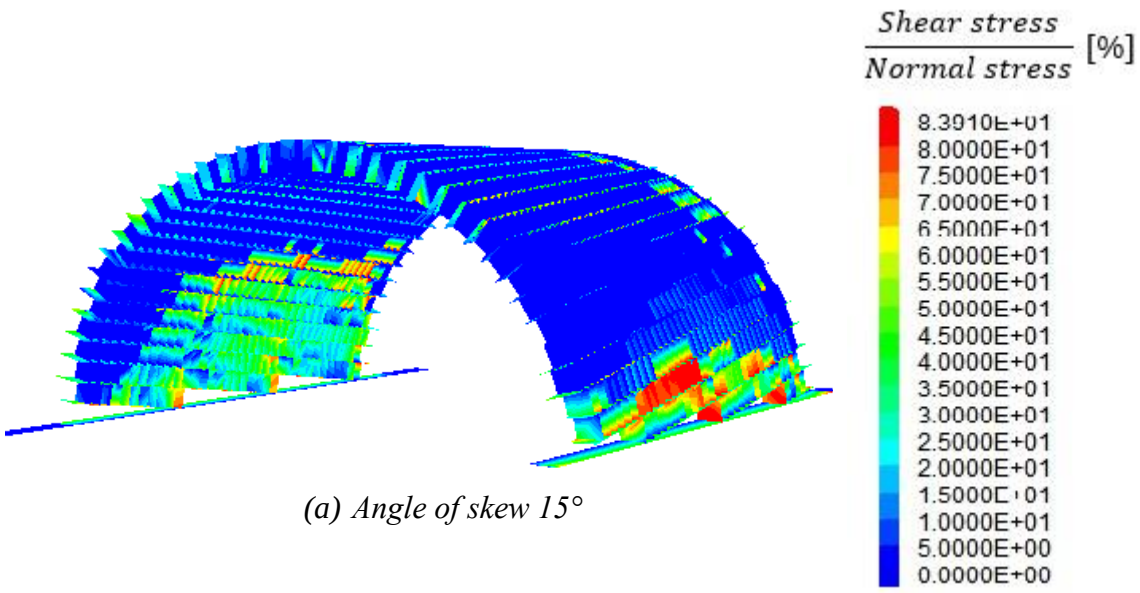

(a) Angle of skew 15°

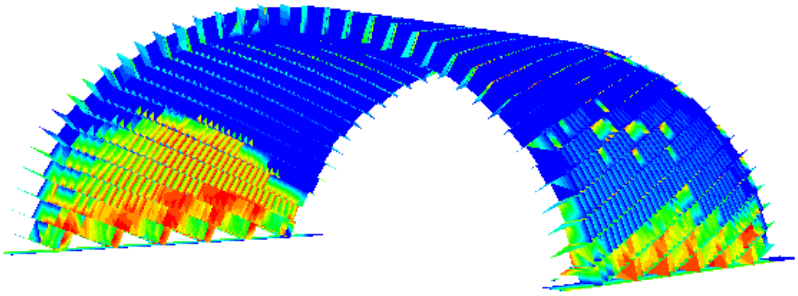

(b) Angle of skew 30°

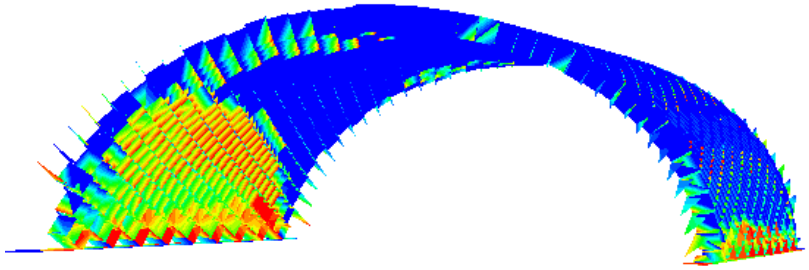

(c) Angle of skew 45°

Figure 30 *– Shear / normal subcontact stress ratio in case of helicoidal method*

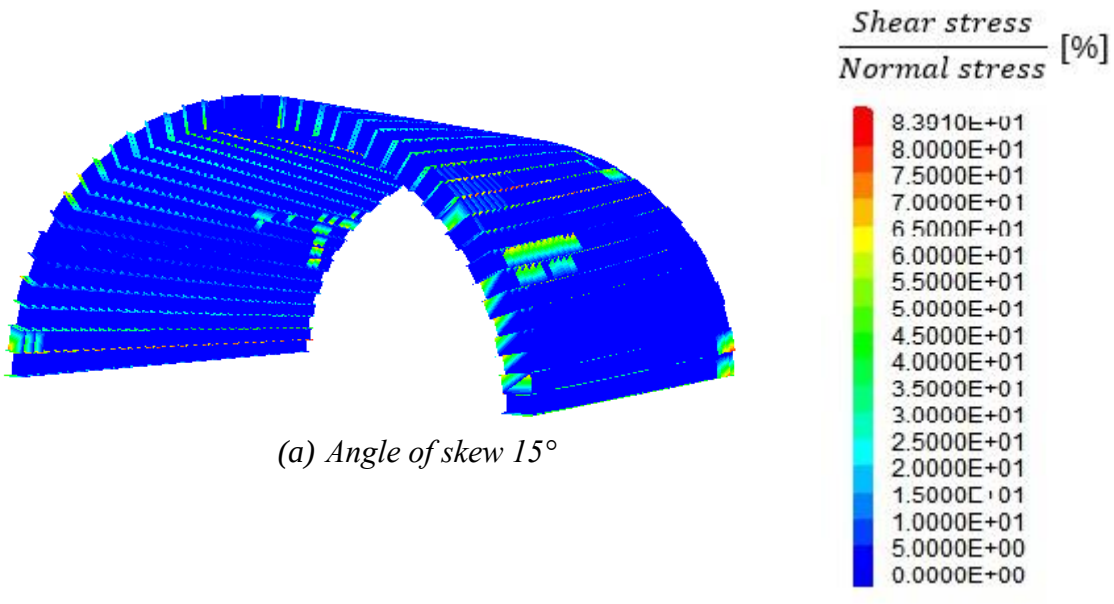

(a) Angle of skew 15°

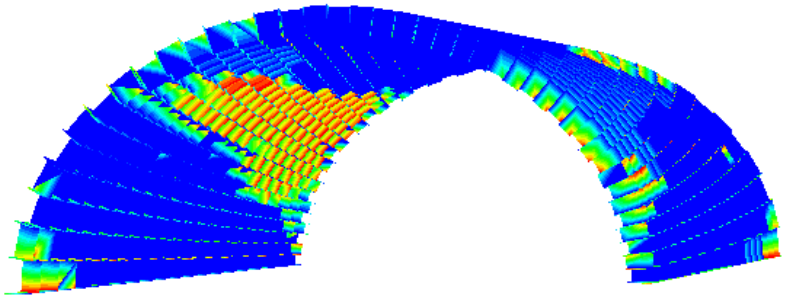

(b) Angle of skew 30°

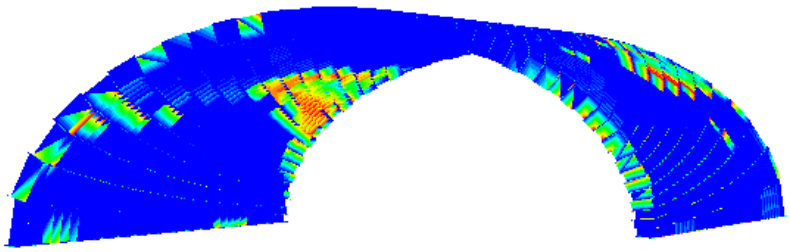

(c) Angle of skew 45°

Figure 31 *- Shear / normal subcontact stress ratio in case of logarithmic method*

8. Conclusions

In this paper, the problem of computing the minimum barrel thickness of semi-circular skewed masonry arches when subjected to their self-weight was investigated. A three-dimension computational model based on the Discrete Element Method (DEM) has been developed. Within DEM, each masonry unit of the arch was represented by a rigid element. Mortar joints were represented as zero thickness interface elements which can open and close according to the magnitude and direction of stresses applied to them. Initially, the model was verified against results obtained from rectangular masonry arches. The numerical simulations provide good agreement with the analytical solution derived by Milankovitch. Then, a sensitivity study was carried out to investigate the minimal barrel thickness with respect to the: a) angle of skew; b) construction method (e.g. false, helicoidal, and logarithmic method); c) size of masonry units; and d) frictional resistance between masonry units. From the results analysis it was found:

- The minimum barrel thickness for a false skew arch increases when the angle of skew increases from 0° to 45°. The helicoidal and logarithmic methods show a different behaviour. With the increasing angle of skew the minimal barrel thickness decreases.
- As the angle of skew and the L/W ratio of the masonry units' increase, the minimum barrel thickness required to sustain the self-weight of the arch decreases.
- The joint friction angle significantly influences the mechanical behaviour of skew arches. From the three investigated construction methods, the false skew arch proved to be the most sensitive to the decrease of frictional resistance below 40°. From ***Figure 27***, the false skew arch does not have that additional resistance due to friction along the "zig-zag" hinge, which is beneficial for helicoidal and logarithmic arches. The biggest difference between the geometry of helicoidal and logarithmic skew arches can be found around the abutments. The helicoidal method shows high shear stresses and the danger of sliding occurs. Presumably this was the reason why the full semi-circular arch constructed according to helicoidal method was avoided (Hyde 1899).

Also, it is concluded that the DEM is an appropriate technique to simulate the collapse of masonry arches. The discrete element method allows for the simulation of rupture phenomenon and thus to manage discontinuities in an elegant and robust way. In the framework of this study there were no attempts to analyse the effect of backfill, spandrel walls or any other construction detail of a masonry arch bridge. It is anticipated that future studies will also include the effect of regulatory live loads.

Acknowledgments

The authors express their gratitude to the ITASCA Education Partnership Program for providing a copy of the 3DEC software to assist the above research. Financial support of the OTKA 100770 project is also gratefully acknowledged.

References

Alexakis, H., Makris, N.; 2013. Minimum thickness of elliptical masonry arches, Acta Mechanica, Vol. 224. Issue 12, pp. 2977-2991.

Bashfort, F., 1855. *Oblique Bridges with Spiral and with Equilibrated Courses.* London: E.andF.N Spon.

BD21/01. Design Manual for Roads and Bridges (DMRB) (2001). Highway structures: Inspection and Maintenance. Volume 3. Part 3:Assessment of Highway Bridges and Structures. London: Highway Agency.

Boothby, T.E., 2001. Analysis of masonry arches and vaults. Progress in Structural Engineering and Materials, Vol. 3, Issue 3, pp.246-256,

Choo, B.S., Gong, N.G. 1995. Effect of skew on the strength of the masonry arch bridges. In Arch Bridges: Proceedings of the First International Conference of Arch Bridges: 205-214. London: Thomas Telford.

Cocchetti, G., Colasante, G. and Rizzi, E., 2011. On the Analysis of Minimum Thickness in Circular Masonry Arches. *Applied Mechanics Review,* Vol. 64.

Couplet, M., 1730. Seconde partie de l'examen de la poussée des voutes, Histoire de l'academie royale de sciences. pp. 117-141.

Cundall, P.A., 1971. A computer model for simulating progressive large scale movements in blocky rock systems. In: Procs. Symposium of the International Society of Rock Mechanics, Nancy, France, 1971, Vol. 1. Paper # II-8.

Cundall, P.A., 1988. Formulation of a three-dimensional distinct element model – Part I: A scheme to detect and represent contacts in a system composed of many polyhedral blocks. International Journal of Rock Mechanics Mining Science, 25(3):107-116.

Cundall, P. and Hart, D., 1992. Numerical modelling of discontinua.. *Journal of Engineering Computations,* Vol. 9, pp. 101-113.

Drosopoulos, G.A., Stavroulakis, G.E., Massalas, C.V., 2006. Limit analysis of a single span masonry bridge with unilateral frictional contact interfaces. Eng. Struct. 28, 1864–1873.

Fanning, P.J., Boothby, T.E., 2001. Three-dimensional modelling and full-scale testing of stone arch bridges. Comput. Struct. 79, 2645–2662.

Foce, F., 2007, Milankovitch's Theorie der Druckkurven: Good Mechanics for Masonry Architecture, Nexus Network J., 9(2), pp.185-210.

Ford, T.E., Augarde, D.E., Tuxford, S.S., 2003. Modelling masonry arch bridges using commercial finite element software. In: 9th International Conference on Civil and Structural Engineering Computing, Egmond aan Zee, 2–4 Sept 2003, The Netherlands.

Fox, C., 1836. On the Construction of Skew Arches. *Architectural Magazine,* Vol.III., pp. 251-260.

Gay, C. 1924 Ponts en macconnerie. J.-B. Bailliére et fils, Paris.

Giamundo, V., Sarhosis, V., Lignola, G.P., Sheng, Y., and Manfredi, G. 2014. Evaluation of different computational modelling strategies for the analysis of low strength masonry structures, Engineering Structures, Volume 73, 160-169, ISSN 0141-0296, http://dx.doi.org/10.1016/j.engstruct.2014.05.007.

Gilbert, M. 1993. The behaviour of masonry arch bridges containing defects. PhD thesis. UK: Manchester University.

Heyman, J., 1966. The Stone Skeleton. *International Journal of Solids and Structures,* Vol. 2., pp. 249-279.

Heyman, J., 1977. *Equilibrium of Shell Structures.* Oxford, UK: Oxford University Press.

Hodgson, J. 1996. The behaviour of skewed masonry arches. PhD thesis. UK: University of Salford.

Hyde, E., 1899. *Skew Arches - Advantages and Disadvantages of Different Methods of Construction.* New York: D. Van Nostrand Company.

ITASCA, 2004. *3DEC - Universal Distinct Element Code Manual. Theory and Background.* Miniapolis: Itasca Consulting Group.

Jiang, K. and Esaki, T., 2002. Qualitative evaluation of stability changes in historical stone bridges in Kagoshima, Japan, by weathering. *Eng. Geol.,* 63., pp. 83-91.

Lemos, J.V., 1995. Assessment of the ultimate load of a masonry arch using discrete elements. In: Middleton, J., Pande, G.N. (Eds.), Computer Methods in Structural Masonry – 3. Books and Journals International, Swansea, UK.

Lemos, J., 2007. Discrete Element Modeling of Masonry Structures. *International Journal of Architectural Heritage,* 1:2., pp. 190-213.

Lemos, J., 2016. *The basis for masonry analysis with UDEC and 3DEC.* IGI Global.

Makris, N., and Alexakis, H. (2013). The effect of stereotomy on the shape of the thrust-line and the minimum thickness of semicircular masonry arches. Archive of Applied Mechanics, 83(10), 1511-1533

Martinez, C., 2012. Application of non-linear finite element analysis to a seven span masonry arch bridge. *Master Thesis UPV.*

Melbourne, C. and Hodgson, J., 1995. *The behaviour of skewed brickwork arch bridges.* Arch Bridges. In: C. Melbourne (editor): Procs. of the First International Conference on Arch Bridges, 3-6 Sept 1995, Bolton, UK

Milankovitch, M., 1907. *Beitrag zur Theorie der Druckkurven. PhD Thesis.* Vienna, Austria: K.K. Technische Hochschule.

Mirabella, R.G., Calvetti, E., 1998. Distinct element analysis of stone arches. In: Sinopoli (Ed.), Arch Bridges; Proc. intern. symp. 6–9 October 1998, Paris, Rotterdam: Balkema.

Nicholson, P., 1828. *A Popular and Practical Treatise on Masonry and Stone-Cutting.* London: Thomas Hurst.

Ochsendorf, J. 2002. Collapse of Masonry Structures, PhD Thesis, University of Cambridge, King's College, UK.

Orbán, Z., 2009. *Calculation methods and diagnostic approaches for historic masonry structures,* Project Report to OTKA, Pécs, Hungary (in Hungarian)

Page, J. 1993. Masonry Arch bridges, TRL State of the Art Review. London: HMSO.

Rankine 1898. A Manual for Civil Engineering, Charles Griffin and Co., London, article 295, pp. 429-432.

Sang, E., 1840. An Essay on the Construction of Oblique Arches. *The Civil Engineer and Architectural Journal,* pp. 232-235.

Sarhosis, V. et. al.., 2013. The behaviour of single span stone masonry skew arches. *7th International Conference on Arch Bridges, Croatia.*

Sarhosis V., Sheng Y. (2014). Identification of material parameters for low bond strength masonry, Engineering Structures, 60, 100-110. DOI: 10.1016/j.engstruct.2013.12.013.

Sarhosis, V., Oliveira, D., Lemos, J. and Lourenco, P., 2014. The effect of skew angle on the mechanical behaviour of masonry arches. *Mechanics Research Communications,* 61., pp. 53-59.

Sarhosis V., Garrity S.W., Sheng Y. (2015). Influence of the brick-mortar interface on the mechanical response of low bond strength masonry lintels, Engineering Structures, 88, 1-11. DOI: 10.1016/j.engstruct.2014.12.014

Sarhosis V., De Santis S., De Felice G. (2016). A review of experimental investigations and assessment methods for masonry arch bridges. Journal of Structure and Infrastructure Engineering, 1, 1-26. DOI:10.1080/15732479.2015.1136655.

Simon J., Bagi K. (2016). DEM analysis of the minimum thickness of oval masonry domes. Int. J. Architectural Heritage 10(4), 457-475

Tóth A., Orbán Z., Bagi K. (2009). Discrete element analysis of a stone masonry arch. Mechanics Research Communications, 36 (4), 469-480

Wang, J., 2004. *The three dimensional behaviour of masonry arches. PhD Thesis.* UK, University of Salford